Climate Dynamics (2026) 64:448
https://doi.org/10.1007/s00382-026-08408-5

ORIGINAL ARTICLE

# Impact of different cloud parameterization scheme combinations in the RegCM4 on the summer climate simulations over China

Fanyu Li[1] · Anning Huang[1,2] · Chunlei Gu[1]

Received: 12 May 2026 / Accepted: 22 September 2026
© The Author(s), under exclusive licence to Springer-Verlag GmbH Germany, part of Springer Nature 2026

**Abstract**
Cloud processes remain a major source of uncertainty in regional climate modeling, this study evaluates the impacts of different combinations of cloud microphysics and cloud fraction schemes on simulations of China's summer climate. Results show the CTRL experiment using RegCM4 with default model configurations clearly overestimates the precipitation and near surface air temperature over most China in summer. Among the four experiments, the SEXPMF experiment coupling the Nogherotto–Tompkins microphysics scheme with the Xu–Randall cloud fraction scheme performs the best to simulate the near surface air temperature and precipitation across most China. Compared to CTRL, SEXPMF reduces the root mean square error (RMSE) of 2-m air temperature (precipitation) simulations by more than 28.4% (14.5%) across all sub-regions of China (in Tibetan Plateau, Northwest and Northeast China), despite the precipitation magnitude is further overestimated in Southeast China, the spatial correlation of simulated precipitation there is increased by 49.0%. Mechanistically, SEXPMF generates more high-level ice clouds, reducing surface downward shortwave radiation and thereby alleviating the widespread warm bias. This fosters an "upper-warming and lower-cooling" vertical thermal structure and enhanced atmospheric stability. Over Tibetan Plateau, this triggers deep anomalous subsidence and moisture divergence, fundamentally suppressing spurious convection and overestimated precipitation. Conversely, the modified thermal field triggers anomalous upper-tropospheric divergence with low-level moisture convergence over Southeast China, leading to strong vertical ascent and favorable cloud formation conditions. However, this ultimately results in over-simulated clouds and excessive precipitation due to compensating errors. This study highlights the critical role of cloud-radiation-dynamic coupling in simulating complex regional climates.

**Keywords** RegCM4 · Cloud parameterization schemes · Summer precipitation and temperature · Radiatively-driven circulation adjustment · China

## 1 Introduction

Regional climate models (RCMs) are key tools for dynamical downscaling, bridging the scale gap between global climate models (GCMs) and local climate characteristics (Rummukainen 2010). RCMs capture mesoscale and regional-scale processes, such as complex topographic effects and land–atmosphere interactions, thereby providing high-resolution information crucial for climate change impact assessments (Giorgi and Gutowski 2015; Liang et al. 2012; Wang et al. 2016; Xu and Yang 2015; Xue et al. 2014). RCMs have been extensively used to investigate the complex climate systems of East Asia (Fu and Yuan 2001; Huang and Zhang 2007; Wang et al. 2003; Yu et al. 2015). However, the performance of RCMs is highly sensitive to the choice of physical parameterization schemes, and no single configuration yields universally optimal performance across different climatic regions (Duan et al. 2017). Moreover, nonlinear interactions among various physical processes significantly influence the simulated climate state (Song et al. 2020), making the evaluation of

✉ Anning Huang
anhuang@nju.edu.cn

✉ Chunlei Gu
chlgu@nju.edu.cn

[1] School of Atmospheric Sciences, Nanjing University, Nanjing 210023, China

[2] Qinghai Lake Comprehensive Observation Research Station, Chinese Academy of Sciences, Gangcha 812300, China

Published online: 06 October 2026

parameterization scheme combinations for specific regions a necessary step to obtain reliable climate projections.

The representation of clouds remains a primary source of uncertainty in current climate simulations, largely due to limited understanding of key physical processes (e.g., Seinfeld et al. 2016) and imperfect model parameterizations (e.g., Khain et al. 2015). Within current cloud parameterizations, cloud microphysics and cloud fraction schemes are two core components. Cloud fraction, as a key macrophysical property affecting radiative transfer and microphysical processes (Wang et al. 2015), directly determines the model's simulation of radiative fluxes (Klein and Hartmann 1993). Cloud microphysics involves microscale interactions among water vapor, aerosols, ice crystals, and precipitation particles, which have profound impacts on large-scale dynamics and long-term climate (Liu et al. 2023; Grabowski et al. 2019; Wang et al. 2022). Deficiencies in understanding cloud processes pose significant challenges to weather and climate modeling (Forster et al. 2021; Morrison et al. 2020; Zelinka et al. 2022). Among the cloud parameterization schemes currently used, cloud microphysics schemes have evolved from simple diagnostic methods to complex prognostic formulations. Early schemes typically diagnosed cloud water content directly based on relative humidity, often lacking a direct simulation of cloud ice (Del Genio et al. 1996). In contrast, modern schemes separate warm and cold cloud physical processes via prognostic equations (Lohmann and Roeckner 1996). The newer Nogherotto–Tompkins scheme explicitly solves prognostic equations for five variables: water vapor, cloud water, rain, cloud ice, and snow, thereby theoretically improving the representation of mixed-phase clouds (Nogherotto et al. 2016).

Cloud fraction parameterization schemes generally fall into two categories: prognostic and diagnostic. Prognostic methods explicitly simulate the temporal evolution of cloud fraction using source and sink terms related to advection, cumulus convection, evaporation, and precipitation (Park et al. 2016; Tiedtke 1993; Tompkins 2002; Wilson et al. 2008), providing a clearer physical basis compared to diagnostic methods. However, each source or sink term in prognostic methods must be parameterized using grid-mean variables, which are difficult to verify directly through observations and involve substantial uncertainty. Conversely, diagnostic methods (e.g., Shiu et al. 2021; Sundqvist et al. 1989; Van Weverberg et al. 2021; Xu and Randall 1996) calculate cloud fraction directly using instantaneous grid-mean atmospheric properties (such as relative humidity and/or cloud water content), offering greater simplicity and efficiency. Although prognostic cloud fraction schemes show slightly better consistency with observations than diagnostic methods (Park et al. 2016; Delanoë et al. 2011), diagnostic methods remain more common in current RCM simulations due to their computational efficiency. With the mainstream adoption of diagnostic schemes that explicitly incorporate cloud water and cloud ice mixing ratios (e.g., Xu and Randall 1996), a direct link is established between macroscopic cloud fraction calculation and microphysical processes, rendering the simulation of cloud fraction highly sensitive to the accuracy of microphysical parameterizations. Consequently, the source/sink terms common in cloud microphysics schemes also depend on the diagnostic results of the cloud fraction scheme. For instance, Desmet et al. (2025) found that in maritime Southeast Asia, the SUBEX scheme combined better with the Xu–Randall scheme than with the newer Nogherotto–Tompkins scheme, resulting in improved performance. Conversely, combining the Nogherotto–Tompkins scheme with the Sundqvist cloud fraction scheme led to increased spurious cloudiness (Nogherotto et al. 2016). This indicates that the impact of different parameterization combinations on model performance varies significantly and is strongly region-dependent. Therefore, evaluating the optimal combination of cloud parameterization schemes for a specific region is critical for optimizing local model performance.

Located in East Asia, China exhibits a pronounced land-sea thermal contrast and Tibetan Plateau (TP) thermal-dynamical forcing, driving a strong East Asian monsoon and substantial spatiotemporal climate variability (Huang et al. 2003; Sha et al. 2015; Yao et al. 2019). Modeling these complex processes requires a sufficiently high horizontal resolution. Currently, a grid spacing of 20–30 km has become a standard configuration for regional climate modeling over this region, as it effectively balances computational feasibility with the ability to represent critical meso-scale phenomena such as the Meiyu front, organized convective systems, and the complex orography of the TP (Gao et al. 2012; Yu et al. 2015). Even at this high-resolution scale, however, regional climate simulation over China remains highly challenging (Gao and Giorgi 2017; Xu et al. 2024). This makes China a highly challenging region for regional climate simulation (Gao and Giorgi 2017; Xu et al. 2024). Although the RegCM system has been widely applied in this region, previous evaluations indicate that the model exhibits persistent systematic biases when using standard configurations. Prominent issues include a significant cold bias of 2-m air temperature simulations in winter and wet bias of precipitation simulations in summer over the TP (Gu et al. 2022, 2024; Luo et al. 2025; Ngo-Duc et al. 2024). These biases are often intrinsically linked to defects in cloud-radiation feedbacks. Some studies suggest that deficiencies in RegCM4's cloud simulation capabilities directly lead to uncertainties in simulated surface downward longwave radiation (SDLR) (Gu et al. 2020; Pareja-Quispe et al. 2021), which in turn may affect precipitation and

temperature simulations. In previous studies, relatively little work has focused on evaluating cloud parameterization schemes specifically for the China region. Existing research has focused more on the entire East Asia region or its subregions, or on other physical processes such as cumulus convection (Chow et al. 2006; Gao et al. 2008, 2012; Zhang et al. 2015). Given the distinct seasonal and spatiotemporal variability of clouds in China (Chen et al. 2012; Shang et al. 2018; Yang et al. 2020), a systematic evaluation of cloud parameterization schemes holds significant scientific value. Therefore, determining the cloud parameterization combination that yields superior performance over China, and clarifying how advanced combinations mitigate local systematic biases by improving the representation of clouds and radiative properties, is a key scientific question that needs to be addressed.

This study utilizes RegCM4 model to conduct four parallel experiments, systematically evaluating the performance of different combinations of microphysics schemes (SUBEX vs. Nogherotto–Tompkins) and cloud fraction schemes (SUBEX vs. Xu–Randall). Specifically, this paper aims to answer three key questions: (1) Among the current mainstream cloud parameterization combinations, which is the optimal choice for regional climate simulation over China? (2) How do different combinations of cloud parameterization schemes affect the simulations of precipitation and surface air temperature in different climatic sub-regions of China? (3) What are the potential physical mechanisms for better cloud parameterization schemes to perform well in these regions?

## 2 Model, cloud schemes, data, experimental design and methods

### 2.1 RegCM4 model

This study employs the Regional Climate Model version 4.5 (RegCM4) developed by the International Centre for Theoretical Physics (ICTP) (Giorgi et al. 2012). As a core tool in the Coordinated Regional Climate Downscaling Experiment (CORDEX), RegCM4 was developed based on the NCAR Mesoscale Model (MM5) framework and includes a comprehensive set of physical parameterization schemes. Its high-resolution capabilities enable detailed climate assessment in regions with complex terrain and facilitate better understanding of underlying physical mechanisms (Berg et al. 2013; Giorgi 2019; Punde et al. 2022). Although RegCM5 was released in 2021, we chose RegCM4 because it remains one of the most widely used regional climate models over East Asia and has been extensively validated in this region (Gao and Giorgi 2017). In contrast, evidence supporting RegCM5's applicability in East Asia remains limited.

### 2.2 Cloud schemes

#### 2.2.1 SUBEX and Xu–Randall cloud parameterization schemes

This section describes the two cloud fraction parameterization schemes of RegCM4. The SUBEX cloud fraction parameterization scheme (Pal et al. 2000) links grid-mean relative humidity with cloud fraction and cloud water content to account for observed subgrid-scale variations. In SUBEX, the cloud fraction ($FC$) is determined by grid-mean relative humidity ($RH$) through the following equation:

$$FC = \sqrt{\frac{RH - RH_{\min}}{RH_{\max} - RH_{\min}}} \tag{1}$$

where $RH_{min}$ represents the relative humidity threshold for cloud formation, and $RH_{max}$ denotes the relative humidity at which $FC$ becomes unity. $FC$ is assumed to be zero when $RH < RH_{min}$ and unity when $RH > RH_{max}$. Typical $RH_{min}$ values vary between 60 and 100%, influenced by factors such as vertical atmospheric level (Sundqvist 1988), surface properties (Sundqvist et al. 1989), and model resolution. However, the SUBEX scheme simplifies this variability by assigning constant $RH_{min}$ values of 80% over land and 90% over ocean, without accounting for vertical temperature dependence. Additionally, the $RH_{max}$ is fixed at 1.01, permitting the water vapor content to surpass saturation by 1%.

The Xu–Randall cloud fraction parameterization scheme (Xu and Randall 1996) incorporates cloud water mixing ratio into cloud fraction prediction, establishing a relationship between subgrid cloud fraction, cloud water mixing ratio, and relative humidity:

$$FC = RH^{\beta}\left[1 - \exp\left(-\frac{\alpha q_c}{[(1 - RH)\, q*]^{\gamma}}\right)\right], RH < 1 \tag{2}$$

$$FC = 1, RH \geq 1 \tag{3}$$

where $q_c$ represents the grid-mean cloud water mixing ratio (sum of cloud ice and liquid water mixing ratios), $RH$ is relative humidity, and $q^*$ denotes the grid-mean saturation mixing ratio. The empirical parameters are set as $\alpha$=100, $\beta$ =0.25, and $\gamma$=0.49. For temperatures below 0 °C, $q^*$ varies between water and ice saturation mixing ratios: it equals the water saturation mixing ratio for pure liquid clouds, ice saturation mixing ratio for pure ice clouds, and their weighted average for mixed-phase clouds.

Notably, unlike the SUBEX scheme, the Xu–Randall scheme incorporates cloud water mixing ratio, which is closely linked to cloud microphysics parameterization. This suggests that different cloud microphysics schemes will influence cloud fraction simulation through their effect on cloud water content.

#### 2.2.2 SUBEX and Nogherotto–Tompkins cloud microphysical schemes

This section describes the two cloud microphysics schemes employed in this study. In the SUBEX scheme (Pal et al. 2000), each model grid is divided into clear and cloudy portions. Any variable $V$ represents the weighted average of its values in the clear ($V_{nc}$) and cloudy ($V_c$) portions, weighted by cloud fraction $FC$:

$$V = FCV_c + (1 - FC)V_{nc} \tag{4}$$

Cloud water is determined by:

$$Q_c = RH - RH_{sat} \tag{5}$$

Rain water is calculated through:

$$P = C_{ppt}(Q_c/FC - Q_c^{th})FC \tag{6}$$

where $1/C_{ppt}$ represents the characteristic time for cloud droplets to convert to rain droplets, $Q_c$ is cloud water, and $Q_c^{th}$ is the autoconversion threshold for cloud water to rain water, scaled according to:

$$Q_c^{th} = C_{acs}10^{-0.49+0.013T} \tag{7}$$

where $T$ is air temperature (°C), and $C_{acs}$ is the autoconversion scale factor, which is empirically set to 0.65 over land and 0.4 over ocean. Notably, SUBEX does not simulate cloud ice, which is a significant limitation of this scheme.

The Nogherotto–Tompkins scheme (Nogherotto et al. 2016) treats cloud ice as a separate prognostic variable and solves predictive equations for rain and snow. It includes four hydrometeors: cloud liquid water, cloud ice, rain, and snow. Each variable is represented by grid-mean mixing ratio $q_x(\mathrm{kg}\cdot\mathrm{kg}^{-1})$. The governing equations for water vapor ($q_v$), cloud water ($q_c$), cloud ice ($q_i$), rain ($q_r$), and snow ($q_s$) mixing ratios are:

$$\frac{Dq_x}{D_t} = S_i + \frac{1}{\rho}\frac{\partial}{\partial z}(\rho V_x q_x) + D \tag{8}$$

where $S_i$ represents the microphysical source and sink terms for each hydrometeor type, indicating water substance conversions between microphysical categories. The second term on the right describes the source of $q_x$ from upper layers due to gravitational sedimentation of species falling at terminal velocity $V_x$. The $D$ term represents any transport or source/sink terms from other parameterized non-adiabatic processes in the model (such as diffusion or deep convection). This recently proposed scheme offers advantages of conservation, computational efficiency, and stability at all time steps, with a numerical solution framework that can be readily extended to include additional microphysical variables.

The key distinction between these schemes lies in their approach: SUBEX employs a classical diagnostic method without cloud ice prediction, potentially leading to simulation errors due to missing ice-phase processes. In contrast, the Nogherotto–Tompkins scheme, as a newly proposed multi-phase prognostic method, offers more comprehensive but computationally complex calculations, with its performance requiring systematic evaluation.

### 2.3 Data

In this study, several observational and reanalysis datasets are utilized to provide initial and lateral boundary conditions for RegCM4 and to serve as benchmark references for evaluating its simulation performance.

To drive RegCM4, the ERA-Interim reanalysis dataset (Dee et al. 2011) from the European Centre for Medium-Range Weather Forecasts (ECMWF), covering the period 1979–2019, is employed to provide the atmospheric initial and lateral boundary conditions. It has a spatial resolution of 1.5° × 1.5°, 37 vertical levels, and a temporal resolution of 6 h. The National Oceanic and Atmospheric Administration (NOAA) Optimum Interpolation Sea Surface Temperature (OISST) weekly dataset (Reynolds et al. 2002), available from 1981 to the present at a spatial resolution of 1° × 1°, is used to provide the oceanic surface boundary conditions.

The ERA5 reanalysis (0.25° × 0.25°; Hersbach et al. 2020), which provides hourly data from 1940 to the present, is used as the benchmark to evaluate the simulated precipitation, 2-m air temperature, circulation, and moisture flux divergence. It provides high-quality, physically consistent meteorological fields through the ECMWF Integrated Forecasting System. Cloud and radiation variables are evaluated using the CLARA-A2 product (Karlsson et al. 2017) from EUMETSAT CM SAF. This satellite-derived dataset has a spatial resolution of 0.25° and spans the period 1982–2015 (with an interim extension to 2019).

## 2.4 Experimental design

To evaluate the performance of different combinations of cloud microphysics and cloud fraction schemes in RegCM4 over China, four experiments were conducted. The CTRL experiment uses the default SUBEX scheme for both cloud microphysics and cloud fraction. The SEXPCM experiment couples the Nogherotto–Tompkins microphysics scheme with the SUBEX cloud fraction scheme, the SEXPCF experiment combines the SUBEX microphysics scheme with the Xu–Randall cloud fraction scheme, and the SEXPMF experiment adopts the coupling of the Nogherotto–Tompkins microphysics scheme and the Xu–Randall cloud fraction scheme.

As shown in Fig. 1, the model domain covers China and its adjacent areas with 400 × 300 grid cells centered at (34° N, 107° E). Consistent with previous studies (Gao et al. 2012; Yu et al. 2015), the model was configured with a horizontal resolution of 20 km. This resolution is capable of resolving large-scale circulation systems as well as the majority of meso-scale weather systems. The domain follows the coverage of the East Asia domain defined by CORDEX (Giorgi et al. 2009), which has been widely used in regional climate simulations over this region and provides adequate representation of the East Asian summer monsoon circulation. The model has 18 vertical levels, with the top at 50 hPa. Following Gu et al. (2022), a dynamic time step of 30 s is used for model integration over the period from 1 May to 31 August of ten summers (2009–2018). The land surface process and solar radiation are calculated every 10 min, the absorption–emission of cloud and gas particles every 18 h, and the cumulus convection together with the dynamic core every 30 s.Lateral boundary conditions are refreshed every 6 h. Surface variables are output hourly, while atmospheric variables are output every 3 h.The first month (May) of each year serves as spin-up and is discarded, leaving only the summer months of June, July, and August for analysis.Additional model configuration details are provided in Table 1.

## 2.5 Methods

To facilitate the subsequent spatial analysis and regional evaluation, the study domain over China is further divided into five sub-regions based on distinct climatic characteristics and topography (Zheng et al. 2010). It is noted that the evaluation and analysis in this study strictly focus on the landmass of China (including Hainan and Taiwan islands), while the surrounding oceanic areas are excluded from the statistical assessment. As illustrated by the solid dividing lines in Fig. 1, the landmass is primarily categorized into five sub-regions: Northwest China (NWC, 73–105° E, 40–49° N), Tibetan Plateau (TP, 73–105° E, 28.5–40° N), Northeast China (NEC, 105–135° E, 40–54° N), Central-East China (CEC, 105–124° E, 28.5–40° N), and Southeast China (SEC, 98–124° E, 18–28.5° N).

To quantitatively assess the model's performance in simulating the climatic mean fields, two standard statistical metrics are employed: the Root Mean Square Error (RMSE) and the spatial Correlation Coefficient (CC) (Wilks 2011).

The RMSE is utilized to measure the absolute magnitude of the average deviation between the simulated results and the observation data. A smaller RMSE value indicates a better agreement in magnitude between the model outputs and the observations. It is calculated as follows:

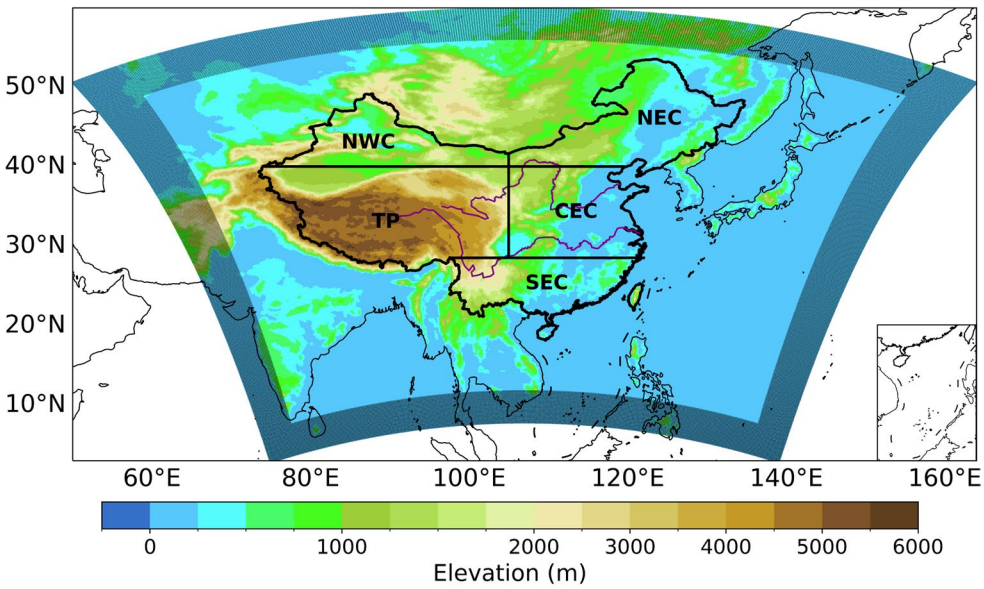



**Fig. 1** Model domain and grid topography at a horizontal resolution of 20 km. Colors indicate terrain elevation (m). Thick solid black lines delineate the five sub-regions used for analysis, with region names labeled inside each box. The analysis in this study focuses exclusively on the terrestrial land areas of China. The buffer zone for lateral boundary relaxation is indicated by the outer grid area. The purple lines represent the Yangtze River and the Yellow River

**Table 1** Model configuration for each experiment

| Items | Values | | | | References |
|---|---|---|---|---|---|
| Experiment name | CTRL | SEXPCF | SEXPCM | SEXPMF | – |
| Cloud microphysics | SUBEX | SUBEX | Nogherotto–Tompkins | Nogherotto–Tompkins | Pal et al. (2000), Nogherotto et al. (2016) |
| Cloud fraction | SUBEX | Xu–Randall | SUBEX | Xu–Randall | Pal et al. (2000), Xu and Randall (1996) |
| Horizontal grids | 400×300 grids centered at (107°E, 34°N) at a horizontal resolution of 20 km | | | | – |
| Terrain dataset | 30″ global DEM (GMTED2010)<br>Bilinearly interpolation and a single pass of 1–2-1 smoothing | | | | – |
| Vertical levels | 18 levels | | | | – |
| Dynamic core | Hydrostatic core | | | | Grell et al. (1994) |
| Radiative transfer model | CCM3 | | | | Kiehl et al. (1998) |
| Planetary boundary layer | Holtslag | | | | Holtslag et al. (1990) |
| Cumulus scheme | Tiedtke over Land, Kain-Fritsch over Ocean | | | | Tiedtke (1989), Kain and Fritsch (1990) |
| Sea flux scheme | Zeng | | | | Zeng et al. (1998) |
| Land surface scheme | CLM4.5 | | | | Oleson et al. (2013) |
| Initial and boundary data | ERA-Interim / NOAA OISST | | | | – |
| Simulation period | From May 1st to August 31st in 2009–2018 | | | | – |
| Analysis period | From June 1st to August 31st in 2009–2018 | | | | – |

$$RMSE = \sqrt{\frac{1}{N}\sum_{i=1}^{N}(S_i - O_i)^2} \tag{9}$$

The spatial Correlation Coefficient (CC) is employed to evaluate the spatial pattern similarity between the simulated and observed fields. CC closer to 1 signifies a higher consistency in the spatial distribution. It is defined as:

$$CC = \frac{\sum_{i=1}^{N}(S_i - \overline{S})(O_i - \overline{O})}{\sqrt{\sum_{i=1}^{N}(S_i - \overline{S})^2 \sum_{i=1}^{N}(O_i - \overline{O})^2}} \tag{10}$$

where $N$ represents the total number of valid grid points over the land area within the evaluated region; $S_i$ and $O_i$ denote the simulated and observed values at the $i$-th grid point, respectively; and $\overline{S}$ and $\overline{O}$ represent the regional spatial averages of the simulation and observation, respectively.

## 3 Model evaluation

As shown in Fig. 2a and b, the CTRL experiment reasonably reproduces the large-scale spatial pattern of precipitation over China, which is characterized by abundant rainfall in the southeast and scarce rainfall in the northwest. It also effectively captures the strong meridional precipitation gradient over eastern China driven by the East Asian summer monsoon. However, a comparison between the CTRL simulation and the ERA5 reference reveals significant systematic biases. Specifically, the model exhibits a pronounced wet bias over the south TP and a distinct dry bias along the southern coast of China.

Furthermore, a widespread systematic warm bias in 2-m air temperature simulation is evident across most of China (Fig. 2c and d). Part of this warm bias over complex terrain may stem from differences in surface elevation between the RegCM4 grid and the ERA5 datasets, as the two systems interpolate topography onto their respective grids using different methods. Nevertheless, this cannot fully explain the systematic nature of the bias. Notably, even over the south of TP, where precipitation is severely overestimated (a condition typically associated with increased cloud cover and cooler temperatures), the warm bias in 2-m air temperature persists. This strongly suggests underlying deficiencies in the model's cloud-radiation feedback mechanisms. Such biases are likely attributable to an underestimation of total cloud fraction or inadequate cloud shielding, which allows excessive solar radiation to reach the surface, thereby driving the systematic warm biases.

As illustrated in the top row of Fig. 3, the CTRL simulation exhibits systematic biases characterized by a pervasive underestimation of stratiform precipitation (Fig. 3a) and a pronounced overestimation of convective precipitation (Fig. 3b). The combined effect of these biases results in a distinct wet bias in total precipitation (Fig. 3c) in most China, particularly over the TP and CEC, alongside a pronounced dry bias over the SEC and the Sichuan Basin.

When modifying only the cloud fraction scheme (the SEXPCF experiment, Fig. 3d), the changes in stratiform precipitation relative to the CTRL experiment are marginal. Conversely, altering the cloud microphysics scheme (the SEXPCM and SEXPMF experiments), the underestimation of stratiform precipitation is alleviated to some extent (Fig. 3j and g), although the magnitude of this change is relatively small compared to that of convective precipitation. Overall, the sensitivity experiments primarily modulate the

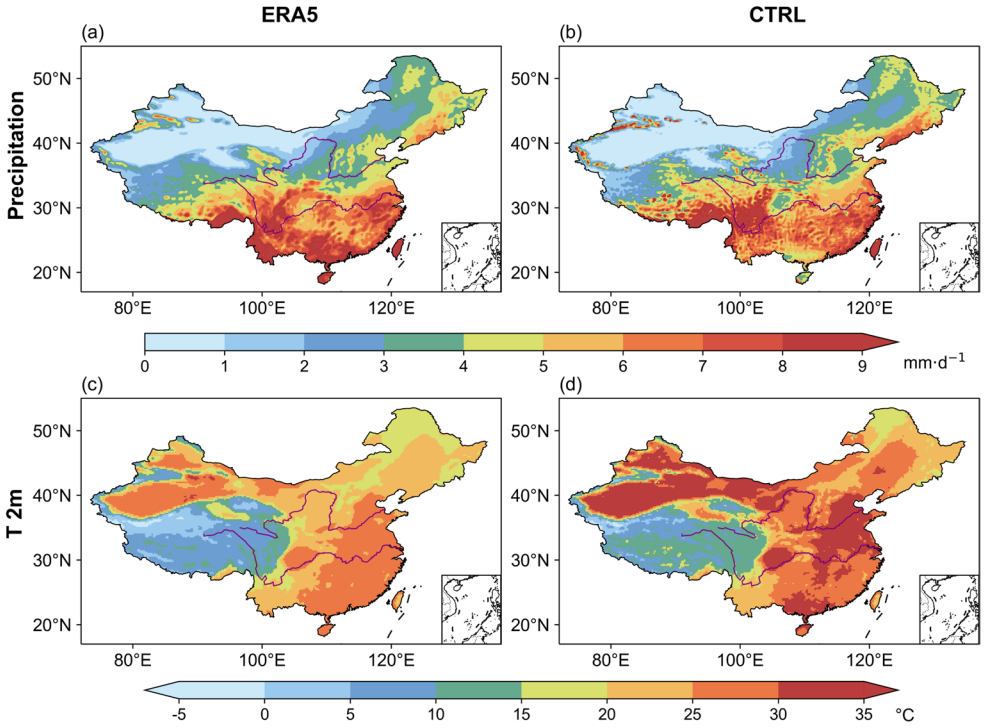



**Fig. 2** The spatial distribution of summer mean precipitation and 2-m air temperature in China from the ERA5 reanalysis and the simulations of the CTRL experiment averaged over 2009–2018. The purple lines represent the Yangtze River and the Yellow River

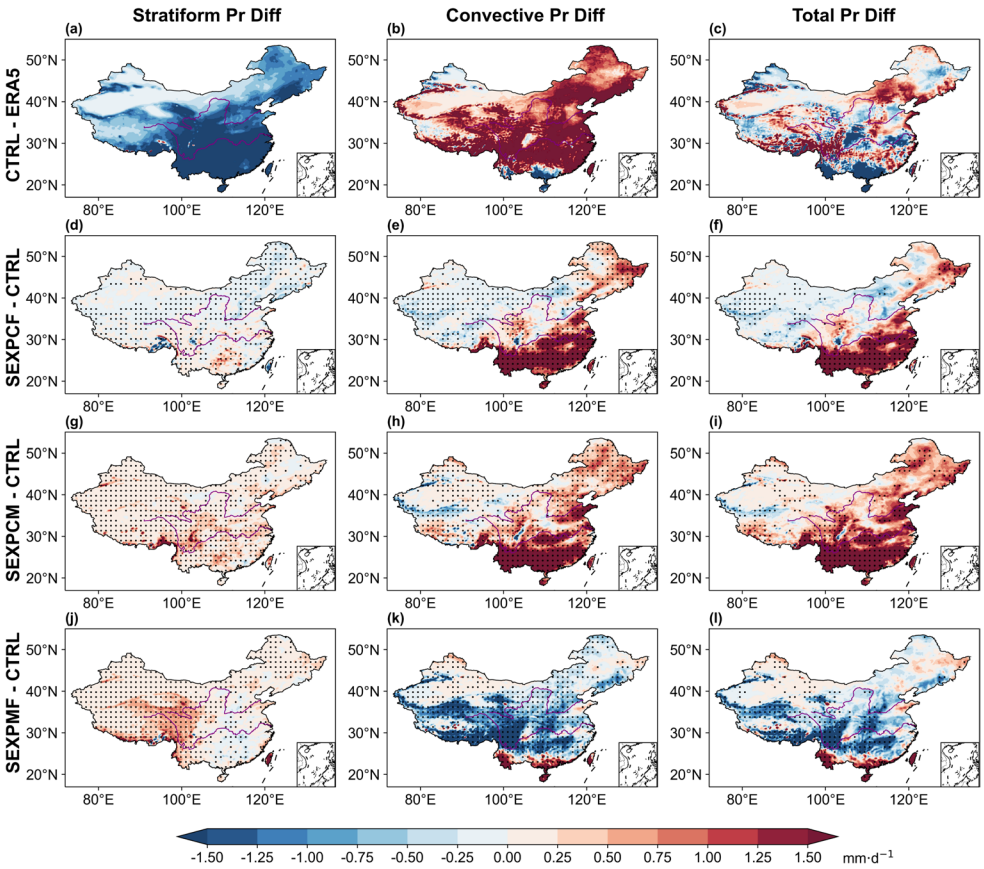



**Fig. 3** Spatial distributions of the differences in summer mean stratiform, convective, and total precipitation over China for the period 2009–2018. The columns from left to right represent stratiform (**a**, **d**, **g**, **j**), convective (**b**, **e**, **h**, **k**), and total precipitation (**c**, **f**, **i**, **l**), respectively. The top row (**a**-**c**) displays the systematic biases of the CTRL experiment relative to the ERA5 reanalysis. The subsequent rows illustrate the differences between each sensitivity experiment and the CTRL experiment (**d**-**l**). Stippling denotes regions where the differences are statistically significant at the 95% confidence level based on Student's t-test. The purple lines represent the Yangtze River and the Yellow River

simulated total precipitation by altering the convective precipitation. Modifying either the microphysics scheme (the SEXPCM experiment) or the cloud fraction scheme (the SEXPCF experiment) individually fails to yield effective improvements in precipitation simulation. In some regions, it even exacerbates the inherent biases of the CTRL experiment (Fig. 3f and i). However, the SEXPMF experiment, which couples the Nogherotto–Tompkins microphysics scheme with the Xu–Randall cloud fraction scheme, demonstrates a unique capability in spatial adjustment (Fig. 3l). Compared to the CTRL experiment, the combined configuration in the SEXPMF experiment significantly reduces the simulated precipitation over most parts of China, particularly over the TP and CEC, although notable over-correction occurs in parts of the CEC. Simultaneously, it generates notable positive differences over the SEC and the Sichuan Basin, substantially alleviating the dry biases in these regions. These results indicate that the SEXPMF experiment can effectively correct the summer precipitation biases over the majority of China.

As shown in Fig. 4a, the CTRL experiment exhibits a pronounced warm bias relative to the ERA5 reanalysis in most China (with positive anomalies exceeding 1.5 °C in majority of the areas). The SEXPCF experiment (Fig. 4b) yields limited improvements in the temperature simulation relative to the CTRL experiment, showing marginal changes overall. In contrast, the SEXPCM experiment (Fig. 4c) manages to alleviate the warm biases in the CTRL experiment to some extent over the high latitudes and the TP (introducing a cooling effect exceeding 1 °C in most of these regions), accompanied by a slight temperature decrease over the SEC. Notably, the SEXPMF experiment (Fig. 4d) produces significant negative temperature differences across the vast majority of China, particularly over the TP and SEC, indicating a substantial reduction in the 2-m air temperature warm bias. This remarkable cooling effect effectively offsets the systematic warming bias inherent in the default configuration of RegCM4.

As shown in Fig. 5a and c, the RMSE of the simulated precipitation clearly demonstrate that the SEXPMF experiment with combined scheme exhibits significant advantages over single-scheme modifications over the TP, NWC, and NEC. In particular, the RMSE of the simulated precipitation in the SEXPMF experiment is reduced by 16.7% and 18.6% relative to the CTRL experiment over the TP and NWC, respectively. However, this experiment yields larger biases than the CTRL experiment over the SEC and CEC, indicating an overcorrection in magnitude despite improvements in the spatial pattern. In terms of spatial correlation, the SEXPMF experiment achieves a remarkable improvement of 49.0% over the SEC (Fig. 5c), effectively correcting the spatial distribution of precipitation in this region. This is consistent with the alleviation of the dry bias over the SEC shown in Fig. 3l.

In contrast, introducing only the cloud fraction scheme in the SEXPCF experiment leads to increased biases of precipitation simulations over most China, particularly over the CEC and SEC (Fig. 5a). Correlation analysis reveals that the SEXPCF experiment improves the spatial pattern of precipitation simulation over the humid regions of China (the SEC, CEC, and NEC) to some extent, with the correlation coefficients increased by 4.1–7.3% (Fig. 5c). Meanwhile, introducing only the cloud microphysics scheme in the SEXPCM experiment causes substantial increases in RMSE

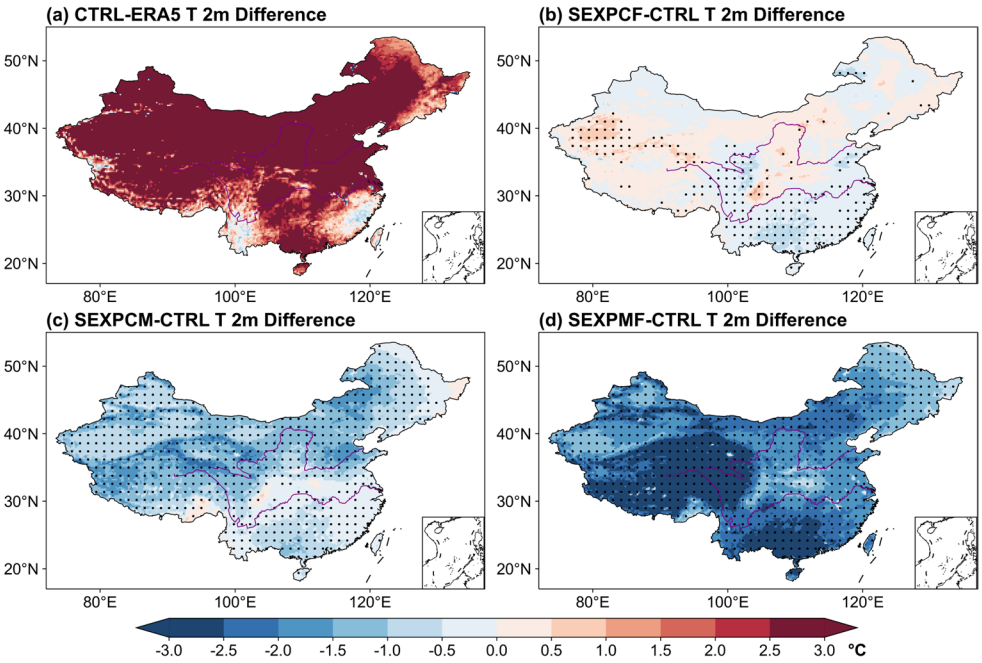



**Fig. 4** Spatial distributions of the biases and differences in the summer mean 2-m air temperature over China averaged over 2009–2018. **a** The systematic bias of the CTRL simulation relative to the ERA5 reanalysis. **b**–**d** The differences between each sensitivity experiment (SEXPCF, SEXPCM, and SEXPMF) and the CTRL. Stippling denotes regions where the differences are statistically significant at the 95% confidence level based on Student's t-test. The purple lines represent the Yangtze River and the Yellow River

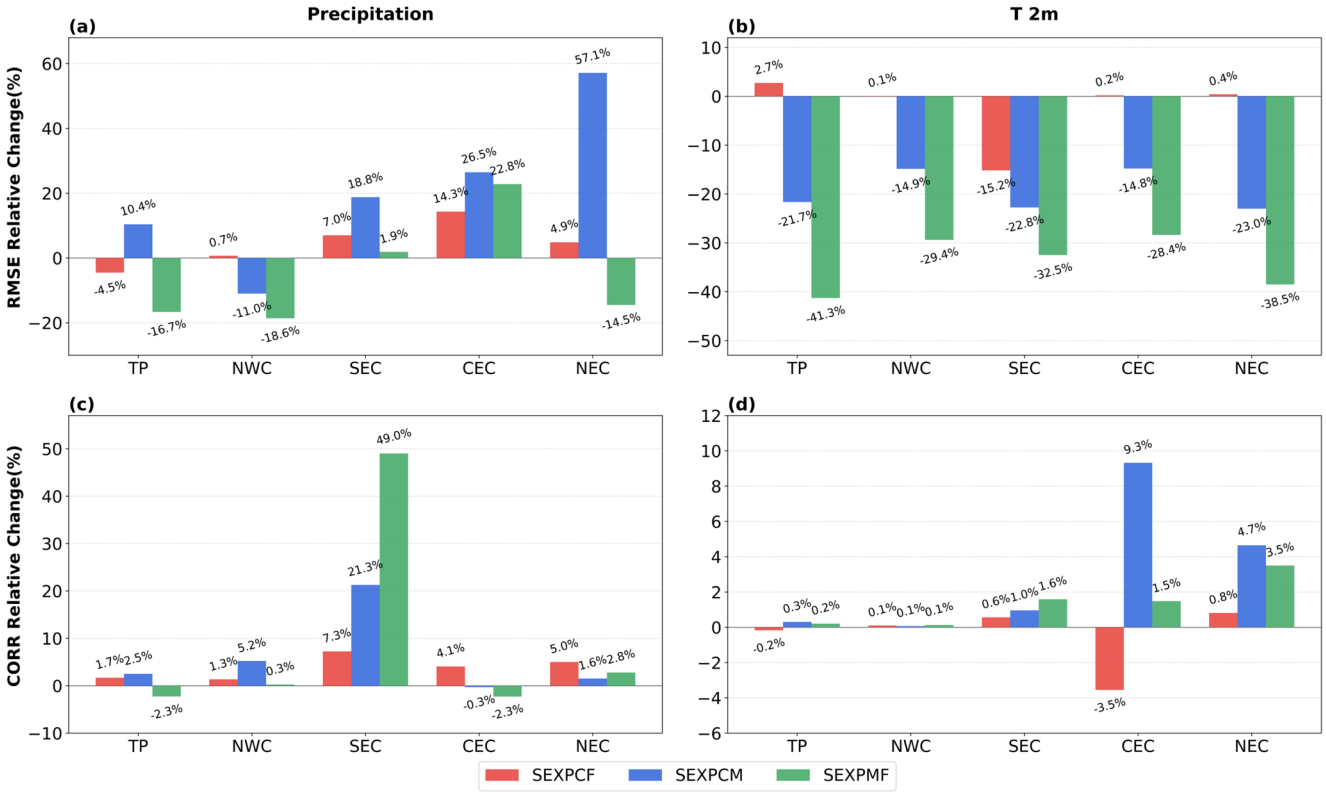



**Fig. 5** Relative changes in the RMSE (**a**, **b**) and spatial correlation coefficient (**c**, **d**) of the climatic mean summer precipitation (**a**, **c**) and 2-m air temperature (**b**, **d**) over each sub-region of China during 2009–2018 simulated by each sensitivity experiment compared to the CTRL experiment

of precipitation simulation over the SEC, CEC, and NEC by 18.8–57.1%, although the spatial correlation coefficients show improvement across all sub-regions (Fig. 5a, c). Overall, modifying a single parameterization scheme leads to a general degradation of precipitation simulation performance over China. Conversely, adopting both schemes simultaneously (the SEXPMF experiment) effectively improves the precipitation simulations over the TP and NWC. Over the SEC, while the absolute precipitation accuracy is reduced, the spatial pattern of the dry bias is substantially improved. However, all three sensitivity experiments underperform in the precipitation simulation over the CEC relative to the CTRL experiment. The performance differences in simulating the 2-m air temperature among the four experiments are more pronounced (Fig. 5b and d): the CTRL experiment produces the largest RMSE in most sub-regions (Fig. 5b), relative to the CTRL experiment, the SEXPMF experiment performs the best in reducing the RMSE of the simulated 2-m air temperature across all sub-regions, with reductions ranging from 28.4 to 41.3% (Fig. 5b). The differences in spatial correlation coefficients among the four experiments are small, though the SEXPMF experiment performs relatively better in the CEC, with an improvement of 9.3% (Fig. 5d).

As a whole, compared to the CTRL experiment, the SEXPCF and SEXPCM experiments generally degrade the simulation performance of summer precipitation over China. Even in specific regions where they show some skill, the improvements are inferior to those of the SEXPMF experiment. The SEXPMF experiment significantly enhances the precipitation simulations in the TP, NWC, and NEC. Simultaneously, it notably refines the spatial pattern of precipitation in the SEC, alleviating the original dry bias (although this may risk an overcorrection that leads to local wet biases). However, the precipitation simulation in the CEC is inferior to that of the CTRL experiment. Regarding temperature simulations, all three sensitivity experiments improve the 2-m air temperature over most China compared to the CTRL experiment. Among them, the SEXPMF experiment yields the largest reductions in RMSE of simulated air temperature across most sub-regions, demonstrating the most pronounced improvement. Comprehensively evaluating the four experiments, the SEXPMF experiment exhibits the best overall performance in simulating the summer precipitation and 2-m air temperature over most China. Therefore, the subsequent analyses will primarily focus on the differences between the simulations of the SEXPMF and CTRL experiments. We will investigate the underlying mechanisms and potential reasons for the impacts of combined cloud

schemes on precipitation and temperature simulations, aiming to provide a robust physical explanation for the changes in model performance.

## 4 Possible mechanisms

### 4.1 Cloud simulation analysis

As illustrated in Fig. 6a, compared to the CLARA observations, the CTRL experiment significantly underestimates the total cloud fraction over China by about 20%. This underestimation partially accounts for the systematic warm bias in the 2-m air temperature (Fig. 4a). Compared to the CTRL experiment, adopting the combination of cloud microphysics and cloud fraction schemes in the SEXPMF experiment clearly improves the simulation of total cloud fraction over most of China (Fig. 6b). Specifically, this experiment significantly increases the cloud cover over the SEC, CEC, and TP, effectively reducing the negative cloud bias inherent in the default model. However, it is worth noting that it may lead to an overestimation of cloud fraction over the SEC.

As shown in Fig. 7a, the SEXPMF experiment, which incorporates the updated cloud microphysics and cloud fraction schemes, produces the total cloud fraction values closest to observations across all five sub-regions. However, it is worth noting that the simulated cloud fraction over the SEC in SEXPMF reaches 74.4%, slightly exceeding the observed value of 72.0%, indicating a positive bias. The SEXPMF experiment exhibits an over-correction of cloud fraction over the SEC (Fig. 7b), which partially explains the significant alleviation of the warm bias in this region (Fig. 4a and d). However, the SEXPMF experiment effectively reduces the negative cloud bias of the CTRL in other sub-regions. The RMSE analysis (Fig. 7c, d) further demonstrates that the SEXPMF experiment significantly improves the simulation of cloud fraction across all sub-regions of China, with the most pronounced improvements over the TP, SEC, and CEC, where the RMSE is reduced by 12.1–50.2%. This broadly corresponds to the regions exhibiting marked temperature improvements in Fig. 4d.

A comparison between the CTRL experiment and ERA5 reanalysis (Fig. 8a–e) reveals the notable deficiencies in the default RegCM4 configuration in representing the vertical structure of clouds. The cloud layers simulated by the CTRL experiment are generally too thin and the simulated coverage of high-level clouds (200–400 hPa) is substantially lower than that in the reanalysis. In contrast, the SEXPMF experiment significantly increases the cloud fraction above 400 hPa across all regions (Fig. 8f–j), with the most pronounced enhancements over the TP (Fig. 8f), SEC (Fig. 8h), CEC (Fig. 8i). Meanwhile, over the CEC and NEC, the SEXPMF experiment effectively reduces the positive bias in low-level clouds inherent in the default configuration. Overall, adopting the combined cloud schemes in the SEXPMF experiment introduces compensating effects that effectively counteract the systematic biases in the CTRL experiment, thereby improving the cloud fraction simulation across various regions. This improvement serves as a fundamental mechanism driving the enhanced simulations of precipitation and 2-m air temperature. However, it is noteworthy that over the SEC and the southern part of CEC, the SEXPMF experiment produces excessively high cloud fraction aloft, with the magnitude of the increase exceeding the initial negative bias between the CTRL experiment and the ERA5 reanalysis. This excessive increase in cloud cover is consistent with the overestimation of precipitation and the marked reduction in 2-m air temperature in this region

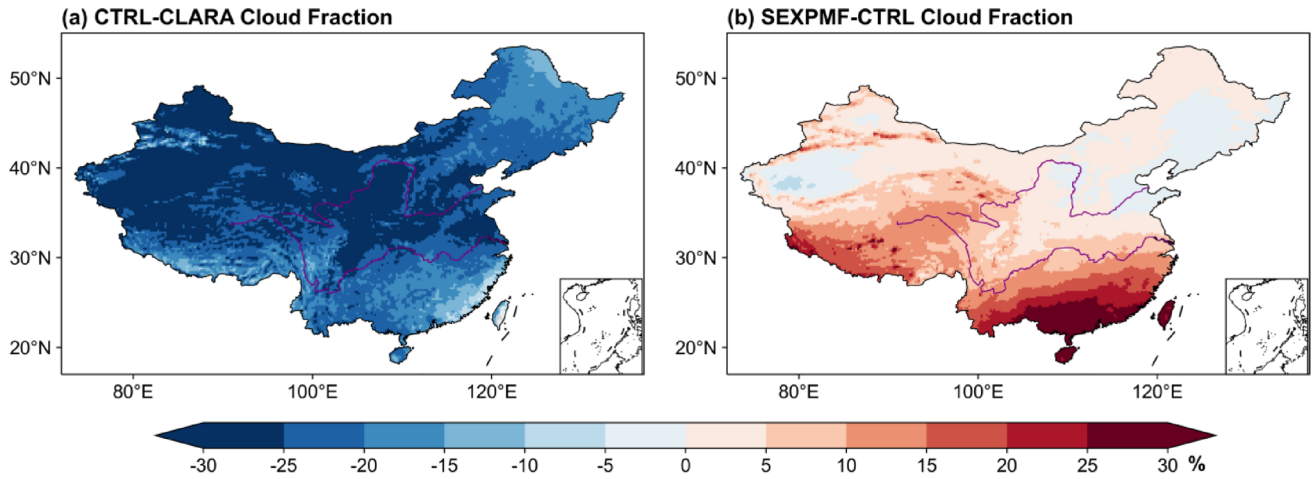
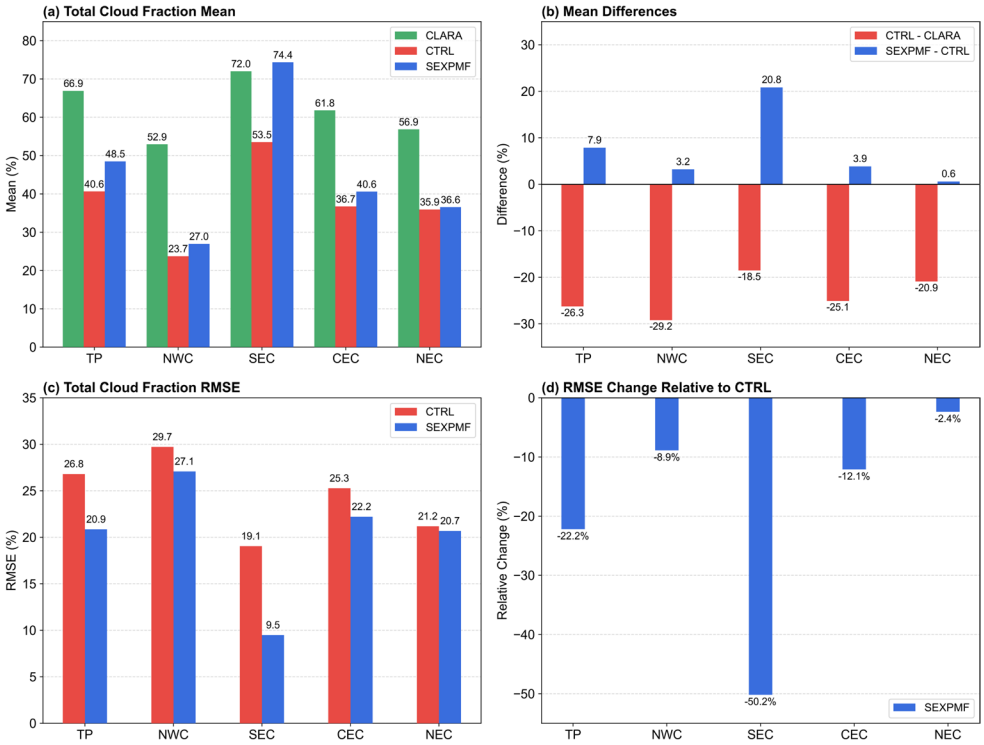



**Fig. 6** Differences in the climatic mean summer total cloud fraction over China during 2009–2018. **a** Difference between the CTRL experiment and CLARA observations (CTRL minus CLARA). **b** Difference between the SEXPMF and CTRL experiments (SEXPMF minus CTRL). The purple lines represent the Yangtze River and the Yellow River



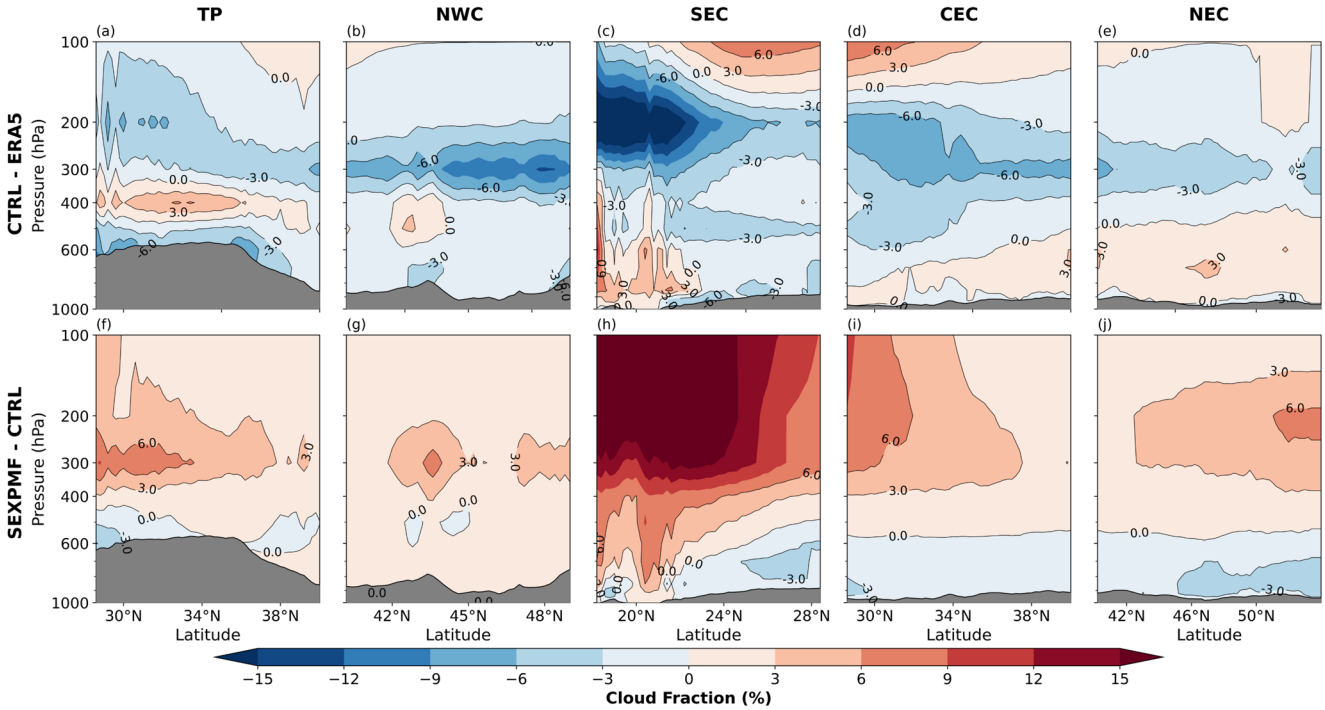




**Fig. 7** Climatic mean summer total cloud fraction, its bias, root mean square error (RMSE), and their relative changes across various sub-regions of China during 2009 −2018. **a** Mean total cloud fraction from the CTRL and SEXPMF experiments. **b** Relative changes in the total cloud fraction bias (CTRL vs. CLARA) and the total cloud fraction (SEXPMF vs. CTRL). **c** RMSE of total cloud fraction for the CTRL and SEXPMF experiments. **d** Changes of the RMSE produced by the SEXPMF experiment relative to the CTRL experiment

**Fig. 8** Latitude-pressure cross sections of the climatic mean summer cloud fraction differences across the five sub-regions in China during 2009–2018. Cloud fraction is zonally averaged across the longitudinal extent of each sub-region, including only the terrestrial land areas of China. The y-axis denotes pressure level, and the x-axis represents latitude. **a**–**e** Differences between the CTRL experiment and ERA5 reanalysis (CTRL minus ERA5). **f**–**j** Differences between the SEXPMF and CTRL experiments (SEXPMF minus CTRL). Note: the ERA5 cloud fraction is model-dependent; satellite products do not currently provide layer-resolved cloud fraction profiles suitable for this analysis

(Figs. 3l and 4d). This suggests that there remains room for further refinement in the combination of SEXPMF experiment, particularly regarding cloud formation mechanisms under the abundant moisture conditions characteristic of the SEC.

To further elucidate the microphysical processes underlying the cloud fraction improvements, Fig. 9 presents the JJA-mean vertical profiles of hydrometeor mixing ratios regionally averaged over China land grid points. The SEXPMF experiment exhibits a distinct reversal in the vertical distribution of total hydrometeors compared to CTRL, specifically an increase in the middle-to-upper troposphere (500–100 hPa) and a decrease in the lower troposphere (below 600 hPa). In the upper troposphere, this increase is dominated by ice-phase hydrometeors (cloud ice and snow), indicating enhanced deposition and freezing processes associated with the Nogherotto–Tompkins scheme. Conversely, the decrease in the lower troposphere is dominated by liquid-phase hydrometeors (cloud water and rain), suggesting enhanced evaporation and melting. The phase transition from liquid to ice occurs primarily between 500 and 600 hPa. This vertical redistribution of hydrometeors suggests a "top-warming, bottom-cooling" microphysical heating structure, characterized by latent heat release from deposition and freezing aloft and cooling from evaporation and melting below. It should be noted that, as the RegCM4 output does not explicitly provide the microphysical heating rate, we utilize the hydrometeor mixing ratios as a proxy to infer these phase-change-related heating effects. This inferred structure remains consistent with the radiative heating profiles and temperature responses discussed in the following section.

Overall, the CTRL experiment with the default configuration exhibits a systematic negative bias in cloud cover simulations over China, primarily attributed to a deficit in high-level clouds. Compared to the CTRL experiment, the SEXPMF experiment simulates greater cloud cover, significantly reducing the RMSE across all sub-regions. This improvement is mainly manifested as an increase in high clouds, particularly over the TP, SEC, and CEC. The underlying physical mechanism for this improvement can be understood from the vertical redistribution of hydrometeors (Fig. 9). When both schemes are actively coupled, the prognostic variables from the Nogherotto–Tompkins microphysics scheme serve as the primary drivers for cloud fraction variations in the Xu–Randall scheme. The SEXPMF experiment produces more ice-phase hydrometeors (cloud ice + snow) in the middle-to-upper troposphere through enhanced deposition and freezing, which directly increases high-level cloud fraction. Meanwhile, the reduction of liquid-phase hydrometeors (cloud water + rain) in the lower troposphere, resulting from enhanced evaporation and melting, contributes to the reduction of excessive low-level clouds over most regions. This coupled mechanism enables a more realistic simulation of cloud fraction and improves its vertical distribution.

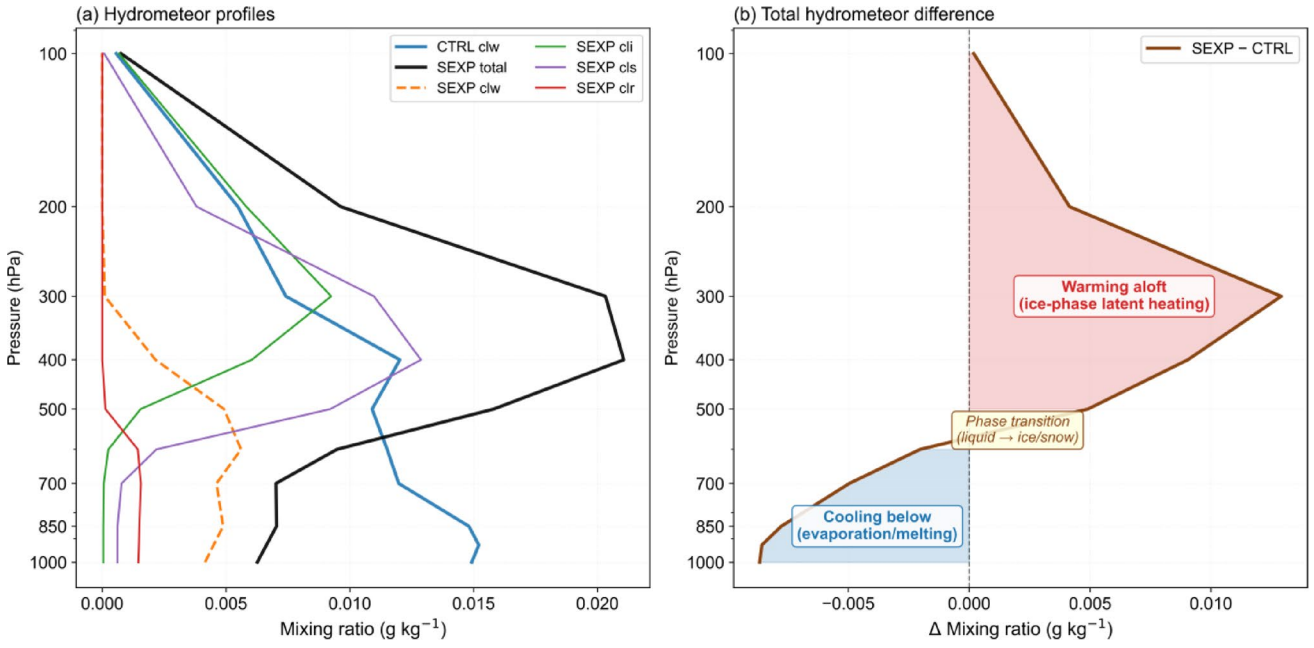



**Fig. 9** JJA-mean vertical profiles of hydrometeor mixing ratios averaged over China land grid points. **a** CTRL (SUBEX scheme; cloud water only) and SEXPMF (Nogherotto–Tompkins scheme; all species). **b** Total hydrometeor difference (SEXPMF minus CTRL). Red (blue) shading indicates increase (decrease). Annotations denote the implied heating structure: warming aloft (ice-phase latent heating), cooling below (evaporation/melting), and the phase transition zone (500–600 hPa)

### 4.2 Radiation and circulation analysis

Figure 10 illustrates the vertical profiles of differences in the summer mean longwave, shortwave, and net radiative heating rates, as well as air temperature across various regions in China. The radiative responses are pronounced across all regions in the SEXPMF experiment. Regarding shortwave radiation (Fig. 10f–j), the SEXPMF experiment generates significant positive heating rates (warming) in the upper atmosphere above 400 hPa, while exhibiting strong negative heating rates (cooling) in the mid-to-lower troposphere below 400 hPa. These changes enhance the albedo of cloud tops, effectively reflecting and absorbing the incoming solar radiation. Consequently, the downward shortwave flux reaching the mid-to-lower troposphere is sharply reduced, thereby cooling the lower atmosphere and the surface. In terms of longwave radiation (Fig. 10a–e), the SEXPMF experiment produces notable positive heating rates in the mid-to-upper troposphere (200–500 hPa). This occurs because the increased high-level ice clouds effectively intercept the upwelling longwave radiation from the lower atmosphere, trapping its energy in the upper troposphere. The net radiative heating rates (Fig. 10k–o) demonstrate that the net effect of the combined scheme is predominantly characterized by a thermodynamic forcing pattern of upper-level warming and lower-level cooling. This vertical distribution can be attributed to the enhanced simulation of high-level cloud systems, increased cloud fraction, and the effective representation of cloud ice in this scheme, consistent with the enhanced ice-phase hydrometeors in the middle-to-upper troposphere shown in Fig. 9.

Correspondingly, the vertical temperature profiles respond to this forcing (Fig. 10p–t), generally exhibiting warming above 400 hPa and cooling below across China. This effect is particularly prominent over the TP, SEC, and CEC. This "upper-warming and lower-cooling" pattern increases the vertical gradient of potential temperature, thereby significantly enhancing the static stability of the atmosphere. This enhanced static stability effectively suppresses the spurious convective activities typically generated by RegCM4 over the TP and other regions, providing a robust thermodynamic explanation for the alleviation of the wet bias of simulated precipitation discussed earlier.

Figure 11 clearly elucidates the critical role of the surface energy budget in modulating model climate biases. The biases of the CTRL experiment simulations reveal that the severe underestimation of cloud fraction in the default configuration (as demonstrated in Fig. 6) leads to insufficient attenuation of incoming solar radiation. Consequently, the surface net shortwave radiation (SNSR, Fig. 11a) exhibits

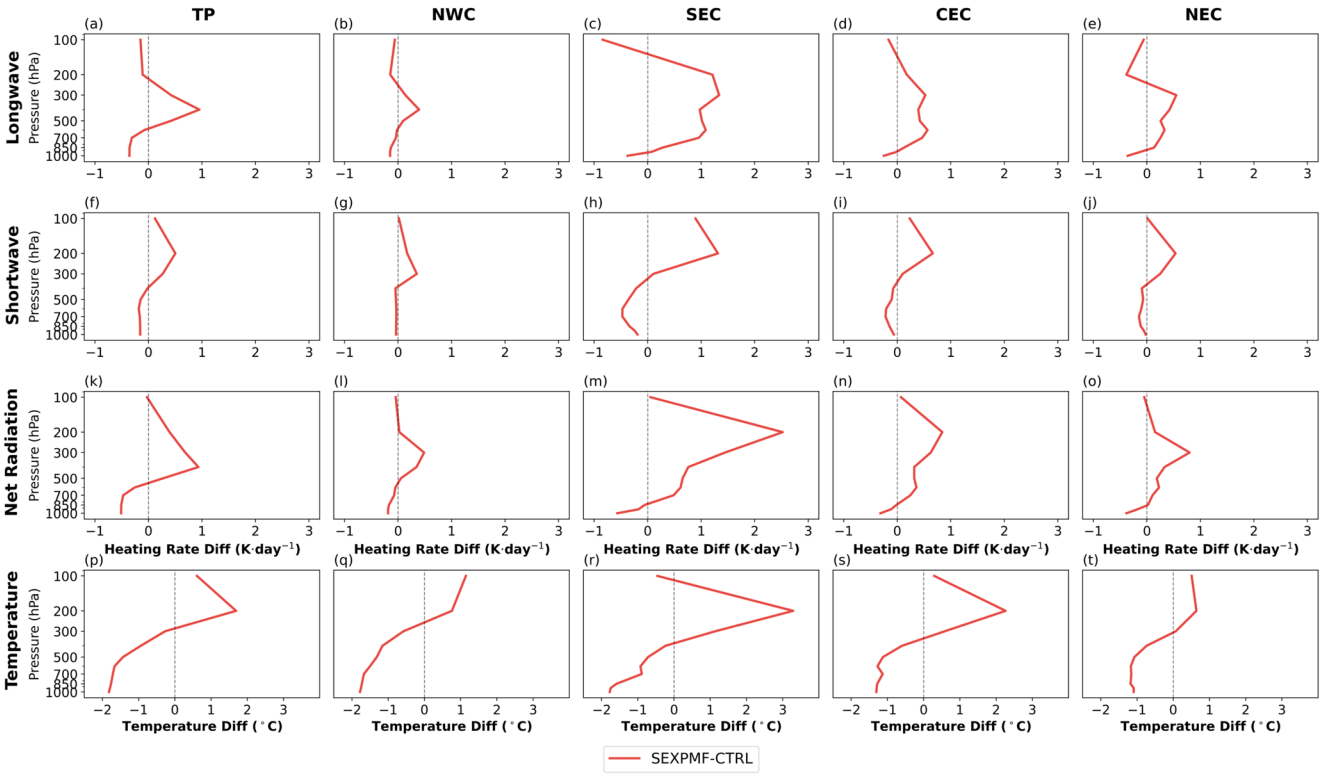



**Fig. 10** Vertical profiles of differences in the climatic mean summer radiative heating rates and air temperature across various sub-regions of China during 2009 to 2018. The y-axis represents the pressure level. The x-axis denotes the heating rate differences (**a**–**o**) and the air temperature differences (**p**–**t**). Differences in the longwave radiative heating rate (**a**–**e**), shortwave radiative heating rate (**f**–**j**), net radiative heating rate (**k**–**o**), and air temperature (**p**–**t**) over each sub-region

massive positive biases (exceeding 50 W $m^{-2}$) over most China, particularly over the SEC and CEC. This excessive downward shortwave radiation dominates the severely overestimated surface net radiation (SNR, Fig. 11e). To balance this surplus in net radiation, the surface releases an excessive amount of sensible and latent heat fluxes (SH+LH, Fig. 11g) into the atmosphere. The exorbitant sensible heat flux directly contributes to the widespread surface warm biases in the CTRL experiment. Concurrently, the excessively high latent heat flux implies overly intense surface evaporation, which injects spurious moisture and unstable energy into the lower troposphere. This is the direct trigger for the overestimated precipitation, especially the spurious convection over the TP.

In contrast, the SEXPMF experiment effectively rectifies this energy imbalance (right column). Because this scheme significantly increases high-level cloud fraction and cloud ice, the strong cloud albedo effect drastically curtails the shortwave radiation reaching the ground. As a result, the SNSR (Fig. 11b) and total SNR (Fig. 11f) in the SEXPMF experiment display widespread and strong negative anomalies. This sharp reduction in surface radiative energy perfectly aligns with the vertical heating rate characteristics of strong cooling in the lower troposphere and at the surface (shown in Fig. 10).

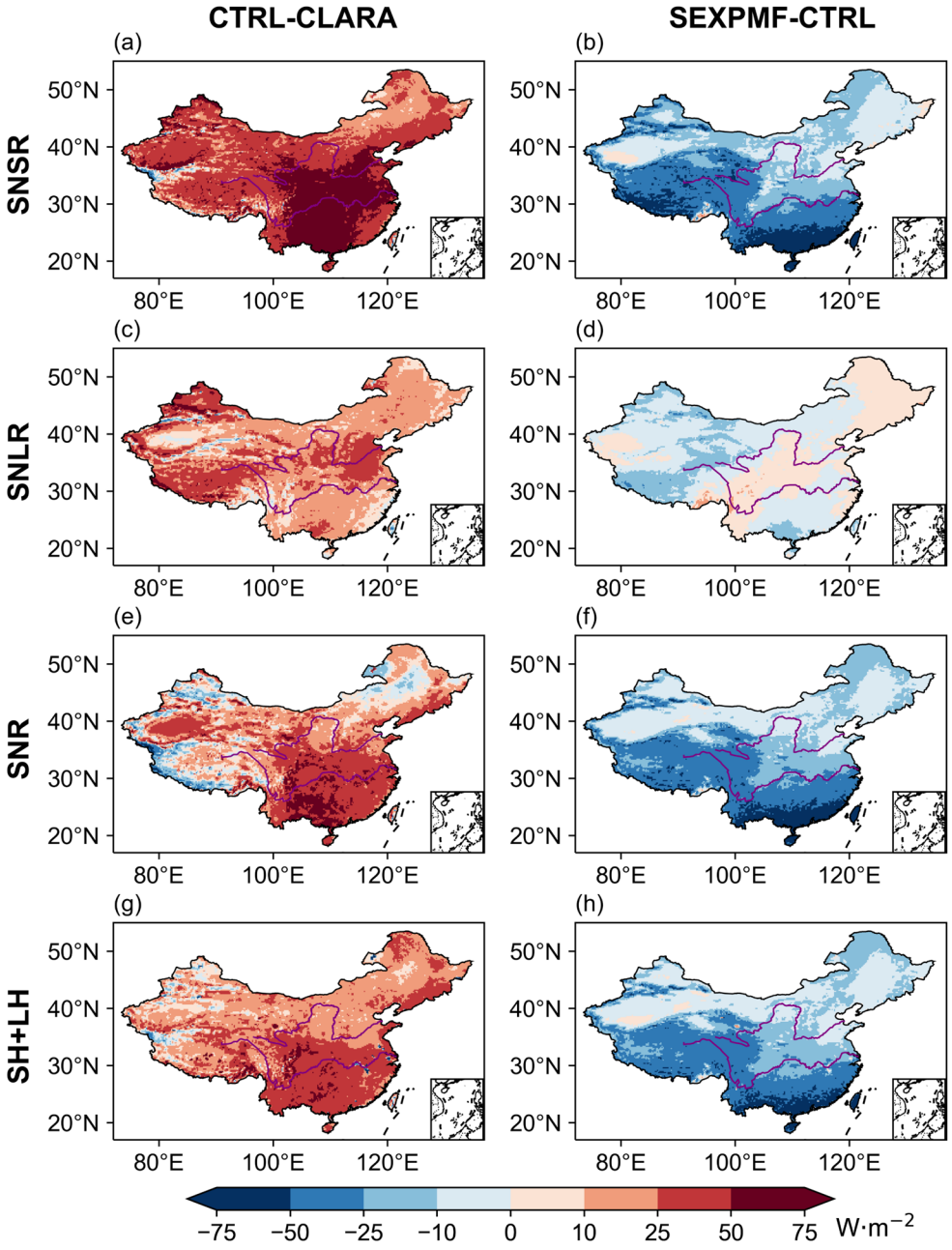



**Fig. 11** Spatial distributions of differences in the climatic mean summer surface radiation balance and heat fluxes in China during 2009–2018. The downward radiative fluxes are defined as positive. The rows, from top to bottom, display the surface net shortwave radiation (SNSR), surface net longwave radiation (SNLR), surface net radiation (SNR), and the sum of surface sensible and latent heat fluxes. The left column shows the differences between the CTRL experiment and the CLARA satellite observations (CTRL minus CLARA), while the right column shows the differences between the SEXPMF and CTRL experiments (SEXPMF minus CTRL). The purple lines represent the Yangtze River and the Yellow River

Driven by the reduced available surface net radiation (SNR), the upward sensible and latent heat fluxes emitted from the surface are correspondingly and substantially diminished in the SEXPMF experiment (Fig. 11h). On one hand, the reduction in sensible heat transport directly cools the surface, effectively alleviating the inherent warm biases. On the other hand, the decrease in latent heat flux weakens surface evaporation, thereby cutting off the moisture supply for spurious precipitation. Particularly over the TP, this reduction in heat fluxes, coupled with the enhanced static stability of the atmosphere (discussed in Fig. 10), decisively suppresses the spurious topographically-induced convection in this region.

However, Fig. 11 also corroborates the earlier concerns regarding "compensating errors" over the SEC. In this region, the SEXPMF experiment induces extremely negative SNSR differences (SEC in Fig. 11b, reaching below $-75$ W m$^{-2}$). This suggests that the marked reduction in surface temperature in this region is essentially achieved at the expense of realistic cloud fraction and radiation budgets. Specifically, the model drives surface cooling by generating excessive clouds to block solar radiation. This further confirms that, under the abundant moisture conditions of the monsoon region, the cloud-radiation feedback mechanisms within the SEXPMF experiment require further calibration.

Figure 12 illustrates the differences of large-scale, three-dimensional adjustments of temperature and circulation between the SEXPMF and CTRL experiments, further uncovering the dynamical mechanisms underlying the alleviation of precipitation biases. The most prominent feature is a robust baroclinic thermodynamic response across the troposphere: in the lower-to-mid troposphere (850 hPa and 500 hPa, Fig. 12a, b), widespread and intense cooling (temperature anomalies reaching $-1$ to $-3$ °C) occurs over most China, accompanied by a distinct cold center over Inner Mongolia. Conversely, in the upper troposphere (200 hPa, Fig. 12c), significant warming (temperature anomalies exceeding + 2 °C) emerges, particularly over the SEC and the TP. This three-dimensional thermal structure is highly consistent with the earlier radiation analysis (Figs. 10 and 11), and specifically corroborates the stronger trapping of upper-level longwave radiation due to the over-simulated cloud fraction in the SEC. This typical "upper-warming and lower-cooling" pattern drastically increases the static stability of the atmospheric column, thereby suppressing vertical convective development.

Driven by these thermal modifications, the large-scale circulation undergoes significant adjustments. The mid-level (500 hPa) cold anomaly over Inner Mongolia, coupled with the upper-level (200 hPa) warming over the SEC, steepens the meridional temperature gradient (Fig. 12b and c). Consistent with the thermal wind relation, this configuration enhances the upper-level westerly flow. Crucially, the SEC is positioned in a region of pronounced anomalous upper-level divergence associated with this accelerated flow. This upper-tropospheric divergence, coupled with the low-level (850 hPa) cyclonic anomaly and convergence over Southern and Southwestern China (Fig. 12a), creates a strong dynamic lifting effect. The resulting vertical coupling serves as the primary dynamical driver for the excessive cloud generation in this region.

In summary, the mechanisms of the combined schemes used in the SEXPMF experiment exhibit a dual nature. On the one hand, the scheme induces a continent-scale upper-warming and lower-cooling structure via cloud-radiation feedbacks, enhancing the static stability and effectively suppressing the prevalent spurious topographically-induced convection. On the other hand, the thermally-induced enhancement of the upper-level jet triggers strong dynamic suction and forced low-level uplift over the SEC. This dynamical feedback mechanism robustly explains the over-simulation of clouds in the SEC and the subsequent "over-corrected" dry bias in precipitation.

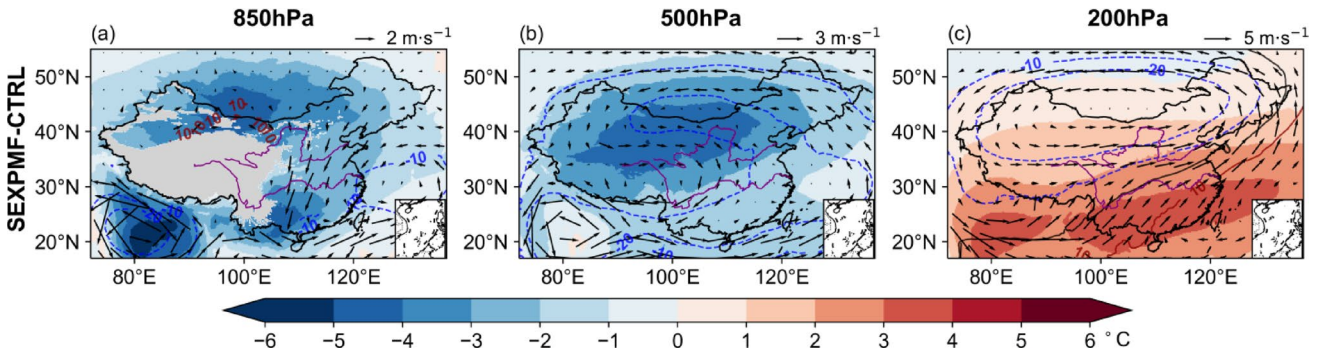



**Fig. 12** Spatial distributions of differences in the climatic mean summer upper-level air temperature and circulation fields between the SEXPMF and CTRL experiments (SEXPMF minus CTRL) over China during 2009–2018. Color shading indicates the air temperature differences, while vectors represent the wind differences. Contours denote the geopotential height differences, with red solid lines and blue dashed lines indicating positive and negative anomalies, respectively. Gray shading indicates the regions masked by topography. The purple lines represent the Yangtze River and the Yellow River

Figure 13 provides the most direct validation of the proposed dynamical suppression and excitation mechanisms by displaying the latitude-pressure cross sections of vertical velocity ($\omega$) differences across the five sub-regions. Note that in pressure coordinates, positive differences indicate anomalous subsidence or weakened ascent, whereas negative differences represent anomalous ascent. The most striking feature appears over the TP (Fig. 13a), where the entire troposphere (from the surface to 200 hPa) is dominated by strong positive anomalies, accompanied by consistent downward anomalous wind vectors. This provides unambiguous physical evidence that the combined schemes used in the SEXPMF experiment suppresses the deep spurious ascending motion triggered by topographic forcing and excessive sensible heat release in the CTRL experiment, by cooling the surface and enhancing the static stability of the atmospheric column (as shown in Figs. 10 and 12). This deep anomalous subsidence constitutes the direct dynamical driver for the fundamental correction of the overestimated precipitation in this region.

In stark contrast to the strong suppression over the TP, the troposphere over the SEC (Fig. 13c) exhibits exceptionally strong negative anomalies penetrating the entire column, coupled with vigorous upward anomalous wind vectors. This prominent feature perfectly corroborates the dynamical mechanism revealed in Fig. 12, namely, the intense dynamic forced uplift driven by upper-level suction over the SEC. This drastic dynamic uplift continuously transports low-level moisture to the upper levels, directly resulting in the over-simulation of clouds in this region. Compared with the dramatic responses over the TP and SEC, the adjustments in vertical motion over the NWC (Fig. 13b), CEC (Fig. 13d), and NEC (Fig. 13e) are relatively modest. In these regions, the variations in vertical velocity are primarily confined to the boundary layer or the lower-to-middle troposphere, exhibiting slight anomalous subsidence or weak alternating

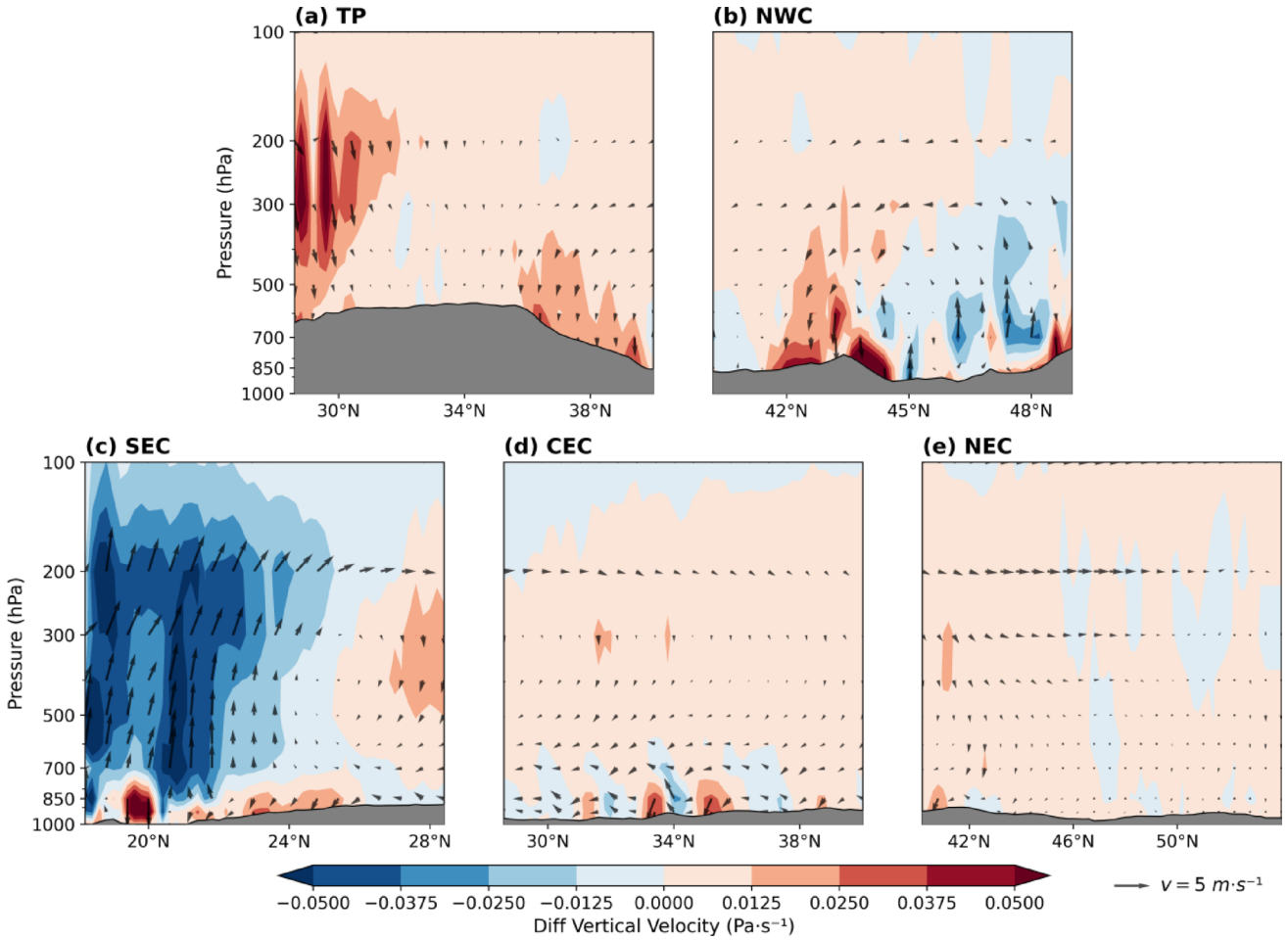



**Fig. 13** Latitude-pressure cross-sections of the differences in the climatic mean summer vertical motion between the SEXPMF and CTRL experiments (SEXPMF minus CTRL) over various sub-regions of China during 2009–2018. Vertical velocity is zonally averaged across the longitudinal extent of each sub-region, including only the terrestrial land areas of China. The y-axis represents the pressure level and the x-axis denotes the corresponding latitude. Color shading indicates the differences in vertical velocity (units: Pa $s^{-1}$). Gray shading represents regions masked by topography. To highlight the vertical motion, the vertical velocity is appropriately scaled up

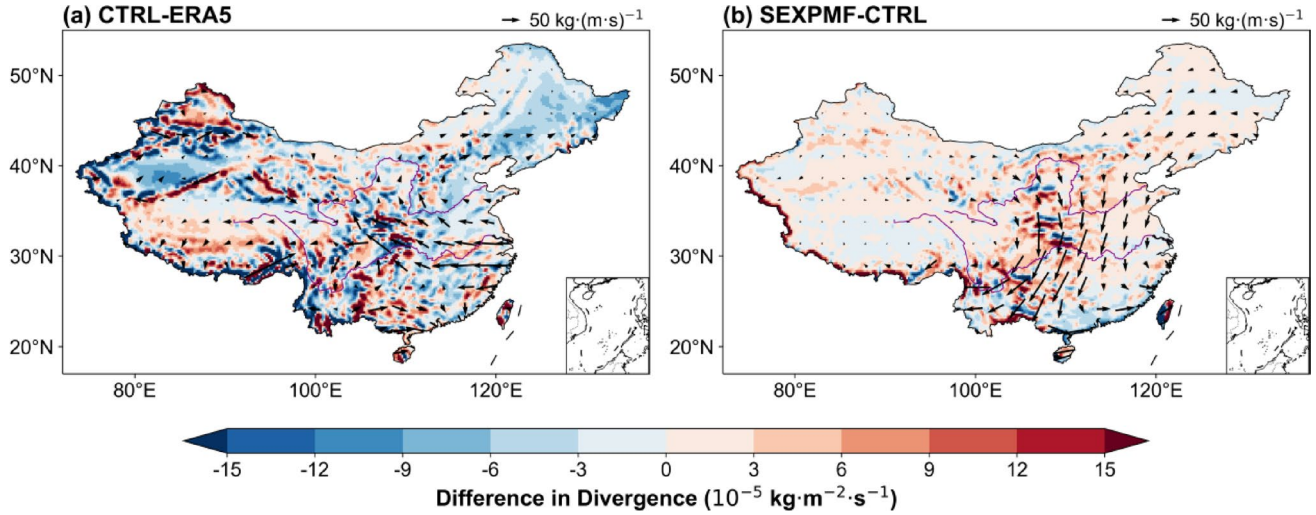



**Fig. 14** Differences in the climatic mean column-integrated (from the surface to 300 hPa) moisture transport flux (vectors) and its divergence (shading) over China in the summers of 2009–2018. **a** Difference between the CTRL experiment and ERA5 reanalysis (CTRL minus ERA5). **b** Difference between the SEXPMF and CTRL experiments (SEXPMF minus CTRL). The purple lines represent the Yangtze River and the Yellow River

perturbations. This indicates that the dynamical impacts of the SEXPMF experiment are relatively mild over these flatter or higher-latitude arid regions, without triggering drastic reorganizations of the vertical circulation.

Figure 14 displays the spatial adjustments in the column-integrated moisture transport flux and its divergence. Initially, in the bias field of the CTRL experiment relative to ERA5 data (Fig. 14a), numerous localized and intense spurious moisture convergence centers exist across the complex topography of the TP and its surrounding areas, which directly correspond to the severe wet precipitation bias originally present in this region. Following the implementation of the SEXPMF experiment (Fig. 14b), the moisture transport field undergoes a significant reorganization. Over the TP, widespread anomalous moisture divergence emerges, accompanied by outward-pointing moisture flux vectors. This adjustment in the moisture field is mutually consistent with the anomalous subsidence revealed in Fig. 13a: the intense dynamical downward motion not only suppresses convection but also forces low-level moisture to diverge outward, cutting off local moisture accumulation. The dual effects of dynamical suppression and reduced moisture supply physically explain why the wet precipitation bias over the Plateau is effectively reduced.

On the other hand, in the SEC and CEC (Fig. 14b), driven by the previously discussed dynamic suction effect, a robust anomalous southwesterly moisture flux continuously surges from the South China Sea into the SEC. This warm and moist airflow induces intense moisture convergence over the SEC and CEC. Concurrently, it is noteworthy that the northward moisture transport from the SEC is suppressed, causing massive amounts of moisture to stagnate and accumulate within the SEC and the southern part of the CEC. The forced dynamic uplift triggered by the accelerated upper-level jet (Fig. 13c), coupled with this exceptionally abundant anomalous moisture convergence (Fig. 14b), provides optimal dynamical and moisture conditions for the generation of upper-level clouds, directly resulting in the overestimation of cloud fraction in this region.

In summary, changes in the vertical distribution of clouds alter the radiative forcing, which in turn drives a systematic reorganization of the large-scale circulation in RegCM4 through thermodynamic-dynamic coupling mechanisms. This constitutes the fundamental physical mechanism by which the SEXPMF experiment improves the spatial distributions of precipitation and surface air temperature. Over the regions such as the TP, the SEXPMF experiment significantly increases the high-level cloud fraction, which substantially reduces the downward shortwave radiation reaching the surface, thereby mitigating the original surface warm bias in the model. Concurrently, the adjusted vertical heating rates foster an anomalous vertical thermal structure of upper-warming and lower-cooling (Fig. 10), dramatically enhancing the static stability of the atmospheric column. This enhanced thermodynamic stability manifests as deep anomalous subsidence throughout the troposphere (Fig. 13). Coupled with the weakened southwesterly moisture transport and enhanced moisture divergence over this region (Fig. 14), this completely cuts off the dynamical and hydrological sources for spurious convection, thereby significantly reducing the wet bias of precipitation simulations. And the modified thermal field reshapes the circulation pattern over the SEC and CEC via hydrostatic balance and the thermal wind relation. The anomalous warm center

at 200 hPa in the south and the cold center at 500 hPa in the north create a robust meridional temperature gradient (baroclinicity), which further accelerates the upper-level southwesterly jet. The SEC is situated beneath the intense upper-level divergence associated with this accelerated jet, generating a profound dynamic suction effect. Coupled with the responsive cyclonic circulation generated at the 850 hPa low level, which excites an intense ascending branch of a secondary circulation, the drastic forced dynamic uplift overcomes the low-level thermodynamic suppression. Furthermore, the moisture transport pathways are subsequently reorganized: moisture transport from the South China Sea into the SEC is significantly enhanced, while its excessive northward transport is suppressed. Consequently, massive amounts of moisture stagnate and converge in the SEC and the South part of the CEC (Fig. 14). This forms a deep zone of dynamic uplift and moisture convergence, providing optimal dynamical and moisture conditions for the generation of the exceptionally abundant upper-level clouds in this region.

## 5 Conclusion

This study systematically evaluated the impacts of four combinations of cloud microphysics and cloud fraction schemes in RegCM4 on summer climate simulations over China during 2009–2018. The main conclusions are summarized as follows.

The SEXPMF, which combines the Nogherotto–Tompkins microphysics with the Xu–Randall cloud fraction parameterization, is identified as the optimal configuration for most regions of China in summer. Compared to the CTRL experiment, SEXPMF reduces the RMSE of 2-m air temperature simulation by more than 28.4% across all five sub-regions of China, and lowers the RMSE of precipitation simulations by over 14.5% in the TP, NWC, and NEC. In the SEC, the spatial distribution pattern is substantially corrected, with the spatial correlation coefficient increased by 49.0%. For CEC, the CTRL experiment retains certain advantages in simulating the precipitation magnitude. It is noteworthy that modifying either the cloud microphysics scheme (SEXPCM) or the cloud fraction scheme (SEXPCF) alone generally degrades the precipitation simulation over China, underscoring the necessity of coupling both advanced schemes for robust performance improvements.

The superior performance of SEXPMF is primarily driven by the enhanced generation of high-level ice clouds, which fundamentally reshapes the surface energy budget and suppresses spurious convection. The synergistic interaction between these two advanced schemes enhances the model's ability to produce high-level ice clouds. Specifically, the improved cloud microphysics module better simulates the partitioning of cloud ice and liquid water characterized by an increase in upper-level cloud ice and a concurrent reduction in low-level liquid water. Furthermore, these refined microphysical quantities serve as inputs for the cloud fraction parameterization, effectively correcting the systematic underestimation of total cloud fraction and optimizing vertical cloud distribution. The consequent increase in high-level cloud cover and ice water content strengthens the reflection of incoming shortwave radiation, significantly reducing downward solar radiation at the surface. This serves as the primary mechanism for alleviating the widespread warm bias in the simulations of 2-m air temperature. More importantly, the resultant vertical thermal structure, which is characterized by upper-tropospheric warming and lower-tropospheric cooling, markedly enhances the atmospheric static stability. In the TP, this enhanced stability triggers deep anomalous subsidence throughout the troposphere, effectively suppressing the spurious convective activity and fundamentally correcting the long-standing overestimation of precipitation.

The cloud-radiation-circulation coupling exhibits pronounced regional dependence and can introduce compensating errors. The modified thermal field establishes a cold anomaly at 500 hPa over northern China and a warm anomaly at 200 hPa over southern China, steepening the meridional temperature gradient and accelerating the upper-level southwesterly jet via the thermal wind relation. SEC becomes situated beneath intense upper-level divergence associated with this accelerated jet, generating profound dynamic suction aloft. Combined with low-level cyclonic convergence and enhanced moisture transport from the South China Sea, this triggers violent ascending motion and excessive moisture convergence. These conditions lead to the overestimation of cloud fraction and precipitation over SEC, revealing a typical "error cancellation" phenomenon: the alleviation of the temperature bias comes partly at the expense of cloud and radiation accuracy. This indicates substantial room for further refinement of cloud system evolution in this region.

In summary, this study identifies the combination of cloud schemes in SEXPMF as the optimal cloud parameterization configuration for RegCM4 over most regions of China, while the default SUBEX scheme retains advantages for precipitation magnitude over the SEC and CEC. The contrasting performances across sub-regions highlight a fundamental challenge in regional climate modeling: no single configuration is universally optimal, and the "error cancellation" phenomenon identified over SEC serves as a cautionary reminder that improvements in one variable may mask deficiencies in another. These findings underscore the value of process-based, multi-variable evaluation

in model development and provide a reference framework for configuring cloud parameterizations in monsoon-dominated regions. Future work could focus on constraining the over-generation of high-level ice clouds under the warm, moisture-rich conditions of the East Asian monsoon, so as to disentangle compensating errors from genuine physical improvements in the SEXPMF. Meanwhile, given the strong coupling between cloud parameterization and other physical processes, examining how the cloud scheme combination in the SEXPMF interacts with different cumulus convection schemes may help clarify the sources of the remaining precipitation biases, particularly over SEC and CEC. A deeper investigation into the microphysical mechanisms behind the superior cloud simulation performance of the SEXPMF over the TP would also be valuable, as understanding its success could offer useful guidance for model development in other high-altitude regions.

**Acknowledgements** Computational resources were provided by the High Performance Computing Center of Nanjing University and the National Key Scientific and Technological Infrastructure project "Earth System Numerical Simulation Facility" (EarthLab). We thank the various agencies for providing data and models.

**Funding** This work was supported by the National Natural Science Foundation of China (Grant U2342207), the Jiangsu Collaborative Innovation Center for Climate Change, the China Postdoctoral Science Foundation (2025M780281), the Postdoctoral Fellowship Program of CPSF (GZC20260160), and the Jiangsu Funding Program for Excellent Postdoctoral Talent under Grant (2026ZB432).

**Data availability** Data—The ERA-Interim reanalysis data (Dee et al. 2011) for lateral boundary conditions, the NOAA Optimum Interpolation Sea Surface Temperature weekly data (Reynolds et al. 2002), the ERA5 reanalysis data (Hersbach et al. 2020), utilized as the reference dataset for precipitation, 2-m air temperature, atmospheric circulation fields, and water vapor flux divergence, the CLARA-A2 cloud products from CM SAF (Karlsson et al. 2017). Software—The Regional Climate Model version 4.5.0 (RegCM v4.5.0) (Giorgi et al. 2012).

## Declarations

**Conflict of interest** The authors declare no conflicts of interest relevant to this study.

## References

Berg P, Wagner S, Kunstmann H, Schädler G (2013) High resolution regional climate model simulations for Germany: Part I—validation. Clim Dyn 40(1–2):401–414. https://doi.org/10.1007/s00382-012-1508-8

Chen H, Yu R, Wu B (2012) FY-2C-derived diurnal features of clouds in the southern contiguous China. J Geophys Res Atmos. https://doi.org/10.1029/2012JD018125

Chow KC, Chan JCL, Pal JS, Giorgi F (2006) Convection suppression criteria applied to the MIT cumulus parameterization scheme for simulating the Asian summer monsoon. Geophys Res Lett. https://doi.org/10.1029/2006GL028026

Dee DP, Uppala SM, Simmons AJ, Berrisford P, Poli P, Kobayashi S, Andrae U, Balmaseda MA, Balsamo G, Bauer P, Bechtold P, Beljaars ACM, van de Berg L, Bidlot J, Bormann N, Delsol C, Dragani R, Fuentes M, Geer AJ, Haimberger L, Healy SB, Hersbach H, Hólm EV, Isaksen L, Kållberg P, Köhler M, Matricardi M, McNally AP, Monge-Sanz BM, Morcrette J-J, Park B-K, Peubey C, de Rosnay P, Tavolato C, Thépaut J-N, Vitart F (2011) The ERA-Interim reanalysis: configuration and performance of the data assimilation system. Q J R Meteorol Soc 137(656):553–597. https://doi.org/10.1002/qj.828

Del Genio AD, Yao M, Kovari W, Lo KK (1996) A prognostic cloud water parameterization for global climate models. J Clim 9(2):270–304. https://doi.org/10.1175/1520-0442(1996)009%3c0270:APCWPF%3e2.0.CO;2

Delanoë J, Hogan RJ, Forbes RM, Bodas-Salcedo A, Stein THM (2011) Evaluation of ice cloud representation in the ECMWF and UK Met Office models using CloudSat and CALIPSO data. Q J R Meteorol Soc. https://doi.org/10.1002/qj.882

Desmet Q, Herrmann M, Ngo-Duc T (2025) Optimizing physical scheme selection in RegCM5 for improved air─sea fluxes over Southeast Asia. Geosci Model Dev 18:8855–8886. https://doi.org/10.5194/gmd-18-8855-2025

Duan Q, Di Z, Quan J, Wang C, Gong W, Gan Y, Ye A, Miao C, Miao S, Liang X, Fan S (2017) Automatic model calibration: a new way to improve numerical weather forecasting. Bull Am Meteorol Soc 98(5):959–970. https://doi.org/10.1175/BAMS-D-15-00104.1

Forster P, Storelvmo T, Armour K, Collins W, Dufresne J-L, Frame D et al (2021) The Earth's energy budget, climate feedbacks, and climate sensitivity. Climate change 2021: the physical science basis. Contribution of Working Group I to the sixth assessment report of the intergovernmental panel on climate change. Cambridge University Press, pp 923–1054. https://doi.org/10.1017/9781009157896

Fu CB, Yuan HL (2001) A virtual numerical experiment to understand the impacts of recovering natural vegetation on the summer climate and environmental conditions in East Asia. Chin Sci Bull 46(14):1199–1203. https://doi.org/10.1007/BF02900602

Gao X, Giorgi F (2017) Use of the RegCM system over East Asia: review and perspectives. Engineering 3(5):766–772. https://doi.org/10.1016/J.ENG.2017.05.019

Gao X, Shi Y, Song R, Giorgi F, Wang Y, Zhang D (2008) Reduction of future monsoon precipitation over China: comparison between a high resolution RCM simulation and the driving GCM: special issue on regional climate studies. Meteorol Atmos Phys 100:73–86. https://doi.org/10.1007/s00703-008-0296-5

Gao X, Shi Y, Zhang D, Wu J, Giorgi F, Ji Z, Wang Y (2012) Uncertainties in monsoon precipitation projections over China: results from two high-resolution RCM simulations. Clim Res 52(1):213–226. https://doi.org/10.3354/cr01084

Giorgi F (2019) Thirty years of regional climate modeling: where are we and where are we going next? J Geophys Res Atmos 124(11):5696–5723. https://doi.org/10.1029/2018JD030094

Giorgi F, Gutowski WJ (2015) Regional dynamical downscaling and the CORDEX initiative. Annu Rev Environ Resour 40:467–490. https://doi.org/10.1146/annurev-environ-102014-021217

Giorgi F, Jones C, Asrar GR (2009) Addressing climate information needs at the regional level: the CORDEX framework. WMO Bull 58(3):175–183

Giorgi F, Coppola E, Solmon F, Mariotti L, Sylla MB, Bi X, Elguindi N, Diro GT, Nair V, Giuliani G, Turuncoglu UU, Cozzini S, Güttler I, O'Brien TA, Tawfik AB, Shalaby A, Zakey AS, Steiner AL, Stordal F, Brankovic C (2012) RegCM4: model description and preliminary tests over multiple CORDEX domains. Clim Res 52:7–29. https://doi.org/10.3354/cr01018

Grabowski WW, Morrison H, Shima S-I, Abade GC, Dziekan P, Pawlowska H (2019) Modeling of cloud microphysics: can we do

better? Bull Am Meteorol Soc 100(4):655–672. https://doi.org/10.1175/BAMS-D-18-0005.1

Grell GA, Dudhia J, Stauffer DR (1994) Description of the fifth generation Penn state/NCAR Mesoscale Model (MM5). Tech Rep. https://doi.org/10.5065/D60Z716B

Gu H, Yu Z, Peltier WR, Wang X (2020) Sensitivity studies and comprehensive evaluation of RegCM4.6.1 high-resolution climate simulations over the Tibetan Plateau. Clim Dyn 54(7):3781–3801. https://doi.org/10.1007/s00382-020-05205-6

Gu CL, Huang AN, Zhang YC, Yang B, Cai SX, Xu XK, Luo JX, Wu Y (2022) The wet bias of RegCM4 over Tibet Plateau in summer reduced by adopting the 3D sub-grid terrain solar radiative effect parameterization scheme. J Geophys Res Atmos. https://doi.org/10.1029/2022JD037434

Gu C, Huang A, Li X, Wu Y (2024) The cold bias in the surface air temperature simulations over the Tibetan Plateau of RegCM4 reduced by adopting the 3D sub-grid terrain longwave radiative effect scheme. J Geophys Res Atmos. https://doi.org/10.1029/2024JD042102

Hersbach H, Bell B, Berrisford P, Hirahara S, Horányi A, Muñoz-Sabater J, Nicolas J, Peubey C, Radu R, Schepers D, Simmons A, Soci C, Abdalla S, Abellan X, Balsamo G, Bechtold P, Biavati G, Bidlot J, Bonavita M, De Chiara G, Dahlgren P, Dee D, Diamantakis M, Dragani R, Flemming J, Forbes R, Fuentes M, Geer A, Haimberger L, Healy S, Hogan RJ, Hólm E, Janisková M, Keeley S, Laloyaux P, Lopez P, Lupu C, Radnoti G, de Rosnay P, Rozum I, Vamborg F, Villaume S, Thépaut J-N (2020) The ERA5 global reanalysis. Q J R Meteorol Soc 146(730):1999–2049. https://doi.org/10.1002/qj.3803

Holtslag AAM, De Bruijn EIF, Pan HL (1990) A high resolution air mass transformation model for short-range weather forecasting. Mon Weather Rev 118(8):1561–1575. https://doi.org/10.1175/1520-0493(1990)118%3c1561:AHRAMT%3e2.0.CO;2

Huang AN, Zhang YC (2007) Impacts of the BATS1e land surface model on the performance of the p-σregional climate model. Chin J Atmos Sci 31(1):155–166. https://doi.org/10.3878/j.issn.1006-9895.2007.01.16

Huang R, Zhou L, Chen W (2003) The progresses of recent studies on the variabilities of the East Asian monsoon and their causes. Adv Atmos Sci 20(1):55–69. https://doi.org/10.1007/BF03342050

Kain JS, Fritsch JM (1990) A one-dimensional entraining/detraining plume model and its application in convective parameterization. J Atmos Sci 47(23):2784–2802. https://doi.org/10.1175/1520-0469(1990)047%3c2784:AODEPM%3e2.0.CO;2

Karlsson K-G, Anttila K, Trentmann J, Stengel M, Fokke Meirink J, Devasthale A, Hanschmann T, Kothe S, Jääskeläinen E, Sedlar J, Benas N, van Zadelhoff G-J, Schlundt C, Stein D, Finkensieper S, Håkansson N, Hollmann R (2017) CLARA-A2: the second edition of the CM SAF cloud and radiation data record from 34 years of global AVHRR data. Atmos Chem Phys 17(9):5809–5828. https://doi.org/10.5194/acp-17-5809-2017

Khain AP, Beheng KD, Heymsfield A, Korolev A, Krichak SO, Levin Z, Pinsky M, Phillips V, Prabhakaran T, Teller A, van den Heever SC, Yano J-I (2015) Representation of microphysical processes in cloud-resolving models: spectral (bin) microphysics versus bulk parameterization. Rev Geophys 53(2):247–322. https://doi.org/10.1002/2014RG000468

Kiehl JT, Hack JJ, Bonan GB, Boville BA, Williamson DL, Rasch PJ (1998) The national center for atmospheric research community climate model: CCM3. J Clim 11(6):1131–1149. https://doi.org/10.1175/1520-0442(1998)011%3c1131:TNCFAR%3e2.0.CO;2

Klein SA, Hartmann DL (1993) The seasonal cycle of low stratiform clouds. J Clim 6(8):1587–1606. https://doi.org/10.1175/1520-0442(1993)006%3c1587:TSCOLS%3e2.0.CO;2

Liang X, Xu M, Yuan X, Ling T, Choi HI, Zhang F, Chen L, Liu S, Su S, Qiao F, He Y, Wang JXL, Kunkel KE, Gao W, Joseph E, Morris V, Yu T, Dudhia J, Michalakes J (2012) Regional climate–weather research and forecasting model. Bull Am Meteorol Soc 93(9):1363–1387. https://doi.org/10.1175/BAMS-D-11-00180.1

Liu Y, Yau M-K, Shima S-I, Lu C, Chen S (2023) Parameterization and explicit modeling of cloud microphysics: approaches, challenges, and future directions. Adv Atmos Sci 40(5):747–790. https://doi.org/10.1007/s00376-022-2077-3

Lohmann U, Roeckner E (1996) Design and performance of a new cloud microphysics scheme developed for the ECHAM general circulation model. Clim Dyn 12(8):557–572. https://doi.org/10.1007/BF00207939

Luo J, Huang A, Jiang X, Xu M, Miao X, Gu C, Zhu X (2025) The cold biases in the soil and surface air temperature simulations of RegCM4.7 model over the Tibetan Plateau in cold seasons reduced by adopting an improved snow cover fraction scheme. J Geophys Res Atmos. https://doi.org/10.1029/2025JD043507

Morrison H, Lier-Walqui MV, Kumjian MR, Prat OP (2020) A Bayesian approach for statistical-physical bulk parameterization of rain microphysics. Part I: scheme description. J Atmos Sci 77(3):1019–1041. https://doi.org/10.1175/JAS-D-19-0070.1

Ngo-Duc T, Nguyen-Duy T, Desmet Q, Trinh-Tuan L, Ramu L, Cruz F, Dado JM, Chung JX, Phan-Van T, Pham-Thanh H, Truong-Ba K, Tangang FT, Juneng L, Santisirisomboon J, Srisawadwong R, Permana D, Linarka UA, Gunawan D (2024) Performance ranking of multiple CORDEX-SEA sensitivity experiments: towards an optimum choice of physical schemes for RegCM over Southeast Asia. Clim Dyn 62(9):8659–8673. https://doi.org/10.1007/s00382-024-07353-5

Nogherotto R, Tompkins AM, Giuliani G, Coppola E, Giorgi F (2016) Numerical framework and performance of the new multiple-phase cloud microphysics scheme in RegCM4.5: precipitation, cloud microphysics, and cloud radiative effects. Geosci Model Dev 9(7):2533–2547. https://doi.org/10.5194/gmd-9-2533-2016

Oleson KW, Lawrence M, Bonan B, Drewniak BA, Huang M, Koven D, Yang Z (2013) Technical description of version 4.5 of the Community Land Model (CLM) (NCAR Technical Note NCAR/TN-503+STR). National Center Atmos Res. https://doi.org/10.5065/D6RR1W7M

Pal JS, Small EE, Eltahir EAB (2000) Simulation of regional-scale water and energy budgets: representation of subgrid cloud and precipitation processes within RegCM. J Geophys Res Atmos 105(D24):29579–29594. https://doi.org/10.1029/2000JD900415

Pareja-Quispe D, Franchito SH, Fernandez JPR (2021) Assessment of the RegCM4 performance in simulating the surface radiation budget and hydrologic balance variables in South America. Earth Syst Environ 5(3):499–518. https://doi.org/10.1007/s41748-021-00249-y

Park R, Chae J, Hong S (2016) A revised prognostic cloud fraction scheme in a global forecasting system. Mon Weather Rev 144(3):1219–1229. https://doi.org/10.1175/MWR-D-15-0273.1

Punde P, Attada R, Aggarwal D, Radhakrishnan C (2022) Numerical simulation of winter precipitation over the Western Himalayas using a weather research and forecasting model during 2001–2016. Climate 10(11):160. https://doi.org/10.3390/cli10110160

Reynolds RW, Rayner NA, Smith TM, Stokes DC, Wang W (2002) An improved in situ and satellite SST analysis for climate. J Clim 15(13):1609–1625. https://doi.org/10.1175/1520-0442(2002)015%3c1609:AIISAS%3e2.0.CO;2

Rummukainen M (2010) State-of-the-art with regional climate models. Wires Clim Change 1(1):82–96. https://doi.org/10.1002/wcc.8

Seinfeld JH, Bretherton C, Carslaw KS, Coe H, DeMott PJ, Dunlea EJ, Feingold G, Ghan S, Guenther AB, Kahn R, Kraucunas I, Kreidenweis SM, Molina MJ, Nenes A, Penner JE, Prather KA, Ramanathan V, Ramaswamy V, Rasch PJ, Ravishankara AR, Rosenfeld D, Stephens G, Wood R (2016) Improving our fundamental understanding of the role of aerosol-cloud interactions

in the climate system. Proc Natl Acad Sci U S A 113(21):5781–5790. https://doi.org/10.1073/pnas.1514043113

Sha Y, Shi Z, Liu X, An Z (2015) Distinct impacts of the Mongolian and Tibetan Plateaus on the evolution of the East Asian monsoon. J Geophys Res Atmos 120(10):4764–4782. https://doi.org/10.1002/2014JD022880

Shang H, Letu H, Nakajima TY, Wang Z, Ma R, Wang T, Lei Y, Ji D, Li S, Shi J (2018) Diurnal cycle and seasonal variation of cloud cover over the Tibetan Plateau as determined from Himawari-8 new-generation geostationary satellite data. Sci Rep 8(1):1105. https://doi.org/10.1038/s41598-018-19431-w

Shiu C-J, Wang Y-C, Hsu H-H, Chen W-T, Pan H-L, Sun R, Chen Y-H, Chen C-A (2021) GTS v1.0: a macrophysics scheme for climate models based on a probability density function. Geosci Model Dev 14:177–204. https://doi.org/10.5194/gmd-14-177-2021

Song T, Huang G, Wang X, Zhou X (2020) Factorial sensitivity analysis of physical schemes and their interactions in Regional Climate Model (RegCM). J Geophys Res Atmos. https://doi.org/10.1029/2020JD032501

Sundqvist H (1988) Parameterization of condensation and associated clouds in models for weather prediction and general circulation simulation. In: Schlesinger ME (ed) Physically-based modelling and simulation of climate and climatic change: Part 1. Springer Netherlands, pp 433–461. https://doi.org/10.1007/978-94-009-3041-4_10

Sundqvist H, Berge E, Kristjánsson JE (1989) Condensation and cloud parameterization studies with a mesoscale numerical weather prediction model. Mon Weather Rev 117(8):1641–1657. https://doi.org/10.1175/1520-0493(1989)117%3c1641:CACPSW%3e2.0.CO;2

Tiedtke M (1989) A comprehensive mass flux scheme for cumulus parameterization in large-scale models. Mon Weather Rev 117(8):1779–1800. https://doi.org/10.1175/1520-0493(1989)117%3c1779:ACMFSF%3e2.0.CO;2

Tiedtke M (1993) Representation of clouds in large-scale models. Mon Weather Rev 121(11):3040–3061. https://doi.org/10.1175/1520-0493(1993)121%3c3040:ROCILS%3e2.0.CO;2

Tompkins AM (2002) A prognostic parameterization for the subgrid-scale variability of water vapor and clouds in large-scale models and its use to diagnose cloud cover. J Atmos Sci 59(12):1917–1942. https://doi.org/10.1175/1520-0469(2002)059%3c1917:APPFTS%3e2.0.CO;2

Van Weverberg K, Morcrette CJ, Boutle I, Furtado K, Field PR (2021) A bimodal diagnostic cloud fraction parameterization. Part I: motivating analysis and scheme description. Mon Weather Rev 149(3):841–857. https://doi.org/10.1175/MWR-D-20-0224.1

Wang Y, Sen OL, Wang B (2003) A Highly Resolved Regional Climate Model (IPRC-RegCM) and Its simulation of the 1998 severe precipitation event over China. Part I: model description and verification of simulation. J Clim 16(11):1721–1738

Wang X, Liu Y, Bao Q, Wu G (2015) Comparisons of GCM cloud cover parameterizations with cloud-resolving model explicit simulations. Sci China Earth Sci 58(4):604–614. https://doi.org/10.1007/s11430-014-4989-y

Wang G, Yu M, Xue Y (2016) Modeling the potential contribution of land cover changes to the late twentieth century Sahel drought using a regional climate model: impact of lateral boundary conditions. Clim Dyn 47(11):3457–3477. https://doi.org/10.1007/s00382-015-2812-x

Wang H, Zhang H, Xie B, Jing X, He J, Liu Y (2022) Evaluating the impacts of cloud microphysical and overlap parameters on simulated clouds in global climate models. Adv Atmos Sci 39(12):2172–2187. https://doi.org/10.1007/s00376-021-0369-7

Wilks DS (2011) Statistical methods in the atmospheric sciences, 3rd; ed. edn. Academic Press

Wilson DR, Bushell AC, Kerr-Munslow AM, Price JD, Morcrette CJ (2008) PC2: a prognostic cloud fraction and condensation scheme. I: scheme description. Q J R Meteorol Soc 134(637):2093–2107. https://doi.org/10.1002/qj.333

Xu K, Randall DA (1996) A semiempirical cloudiness parameterization for use in climate models. J Atmos Sci 53(21):3084–3102. https://doi.org/10.1175/1520-0469(1996)053%3c3084:ASCPFU%3e2.0.CO;2

Xu Z, Yang Z (2015) A new dynamical downscaling approach with GCM bias corrections and spectral nudging. J Geophys Res Atmos 120:3063–3084. https://doi.org/10.1002/2014JD022958

Xu H, Liang X, Xue Y (2024) Regional climate modeling to understand Tibetan heating remote impacts on East China precipitation. Clim Dyn 62:2683–2701. https://doi.org/10.1007/s00382-022-06266-5

Xue Y, Janjic Z, Dudhia J, Vasic R, De Sales F (2014) A review on regional dynamical downscaling in intraseasonal to seasonal simulation/prediction and major factors that affect downscaling ability. Atmos Res 147:68–85. https://doi.org/10.1016/j.atmosres.2014.05.001

Yang Y, Zhao C, Fan H (2020) Spatiotemporal distributions of cloud properties over China based on Himawari-8 advanced Himawari imager data. Atmos Res 240:104927. https://doi.org/10.1016/j.atmosres.2020.104927

Yao Y, Zou X, Zhao Y, Wang T (2019) Rapid changes in land-sea thermal contrast across China's coastal zone in a warming climate. J Geophys Res Atmos 124(4):2049–2067. https://doi.org/10.1029/2018JD029347

Yu E, Sun J, Chen H, Xiang W (2015) Evaluation of a high-resolution historical simulation over China: climatology and extremes. Clim Dyn 45(7):2013–2031. https://doi.org/10.1007/s00382-014-2452-6

Zelinka MD, Klein SA, Qin Y, Myers TA (2022) Evaluating climate models' cloud feedbacks against expert judgment. J Geophys Res Atmos 127(2):e2021JD035198. https://doi.org/10.1029/2021JD035198

Zeng X, Zhao M, Dickinson RE (1998) Intercomparison of bulk aerodynamic algorithms for the computation of sea surface fluxes using TOGA COARE and TAO Data. J Clim 11(10):2628–2644

Zhang D, Gao X, Ma J (2015) Analysis of summer climate over China from hindcast experiments by CCSM4.0 and RegCM4.4 models. Clim Environ Res 20(3):307–318. https://doi.org/10.3878/j.issn.1006-9585.2015.14158

Zheng JY, Yin YH, Li BY (2010) A new scheme for climate regionalization in China. Acta Geogr Sin 65(1):3–12

**Publisher's Note** Springer Nature remains neutral with regard to jurisdictional claims in published maps and institutional affiliations.

Springer Nature or its licensor (e.g. a society or other partner) holds exclusive rights to this article under a publishing agreement with the author(s) or other rightsholder(s); author self-archiving of the accepted manuscript version of this article is solely governed by the terms of such publishing agreement and applicable law.